Evolution of Cosmological Magnetic Fields from Early to Late Times

Tina Kahniashvili

Bernoulli Program:
Generation, evolution, and observations of cosmological magnetic fields

May 6 2024

outline

- looking backward – primordial magnetic fields
- modeling and constraints
- evolution from the early to the late universe

collaboration

- Axel Brandenburg, Leonardo Campanelli, Ruth Durrer, Giga Gogoberidze, Arthur Kosowsky, Andrii Neronov, Bharat Ratra, Alexander Tevzadze, Tanmay Vachaspati
- Emma Clarke, Claire Huang, Andrew. Mack, Sayan Mandal, Salome Mtchedlidze, Alberto Roper Pol, Jonathan Stepp, Guitong Sun, Winston Yin
- Andrew Long, Philip Mocz, Jennifer Schober, Mark Vogelberger…

brief history of the universe

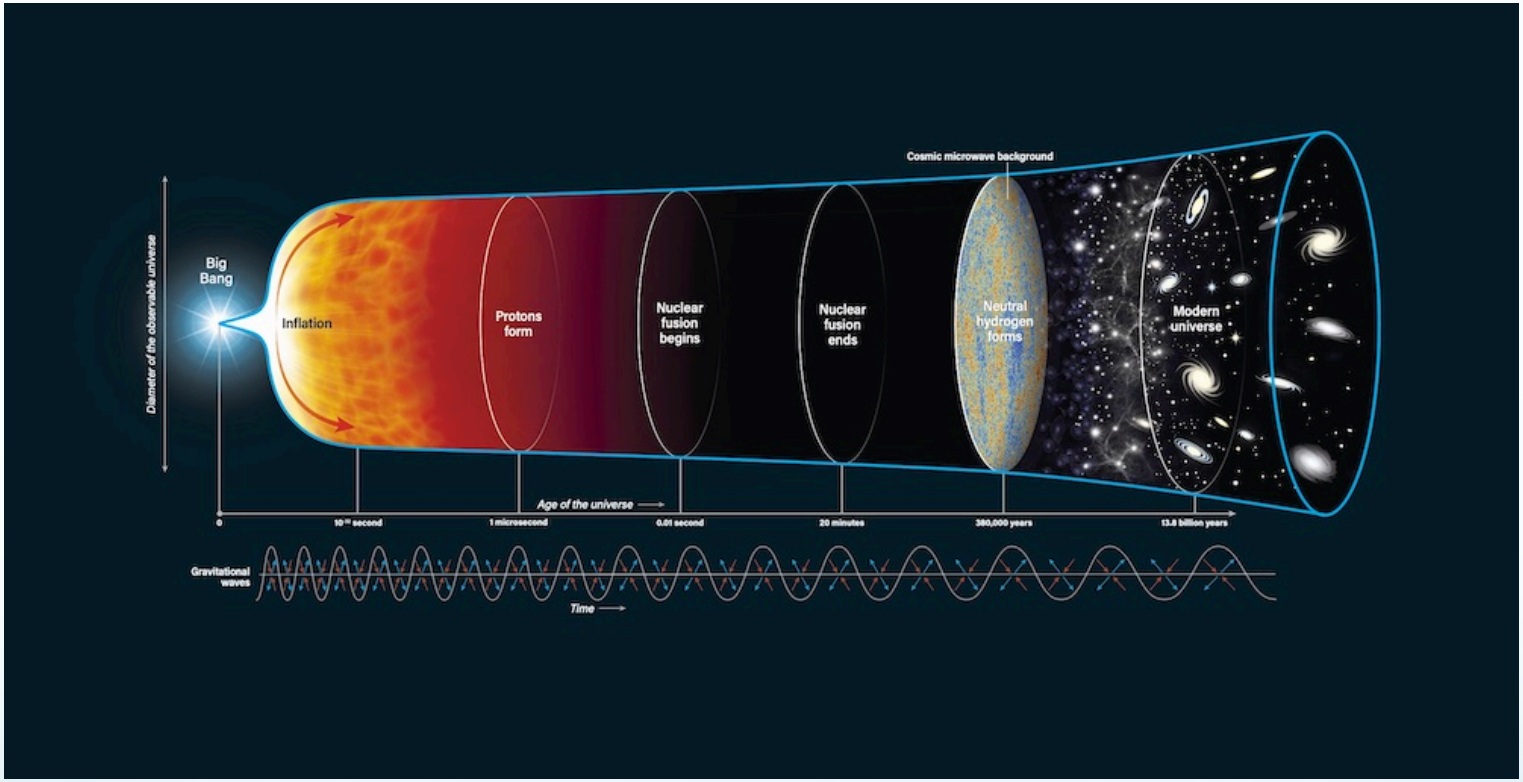

https://astronomy.com/magazine/news/2021/01/the-beginning-to-the-end-of-the-universe-inflating-the-universe

cosmic magnetic fields

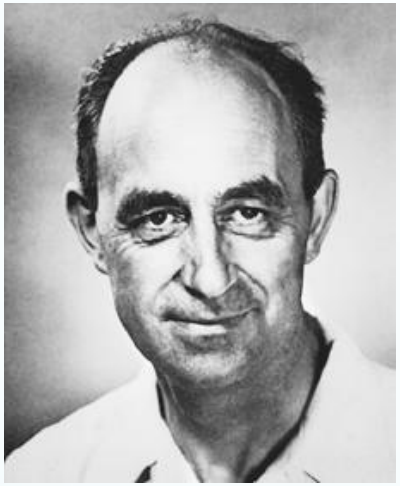

E. Fermi
***"On the origin of the cosmic radiation"*,**
PRD, 75, 1169 (1949)

PHYSICAL REVIEW VOLUME 75, NUMBER 8 APRIL 15, 1949

On the Origin of the Cosmic Radiation

ENRICO FERMI
Institute for Nuclear Studies, University of Chicago, Chicago, Illinois
(Received January 3, 1949)

A theory of the origin of cosmic radiation is proposed according to which cosmic rays are originated and accelerated primarily in the interstellar space of the galaxy by collisions against moving magnetic fields. One of the features of the theory is that it yields naturally an inverse power law for the spectral distribution of the cosmic rays. The chief difficulty is that it fails to explain in a straightforward way the heavy nuclei observed in the primary radiation.

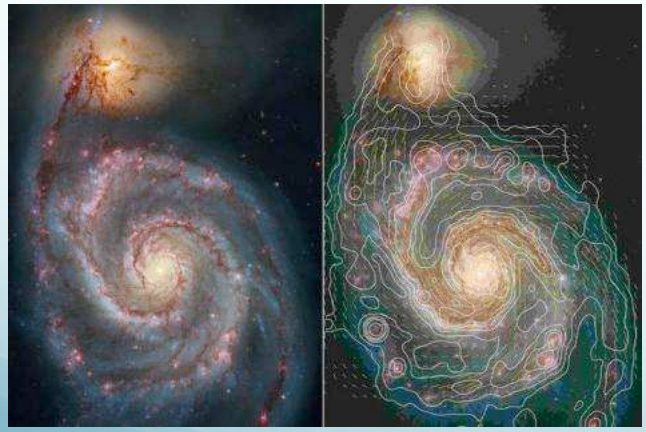

F. Hoyle
in Proc. "*La structure et l'evolution de l'Universe*"
(1958)

https://phys.org/news/2011-05-cosmic-magnetic-fields.html

primordial magnetogenesis

- inflation
- phase transitions
- supersymmetry
- string cosmology
- topological defects

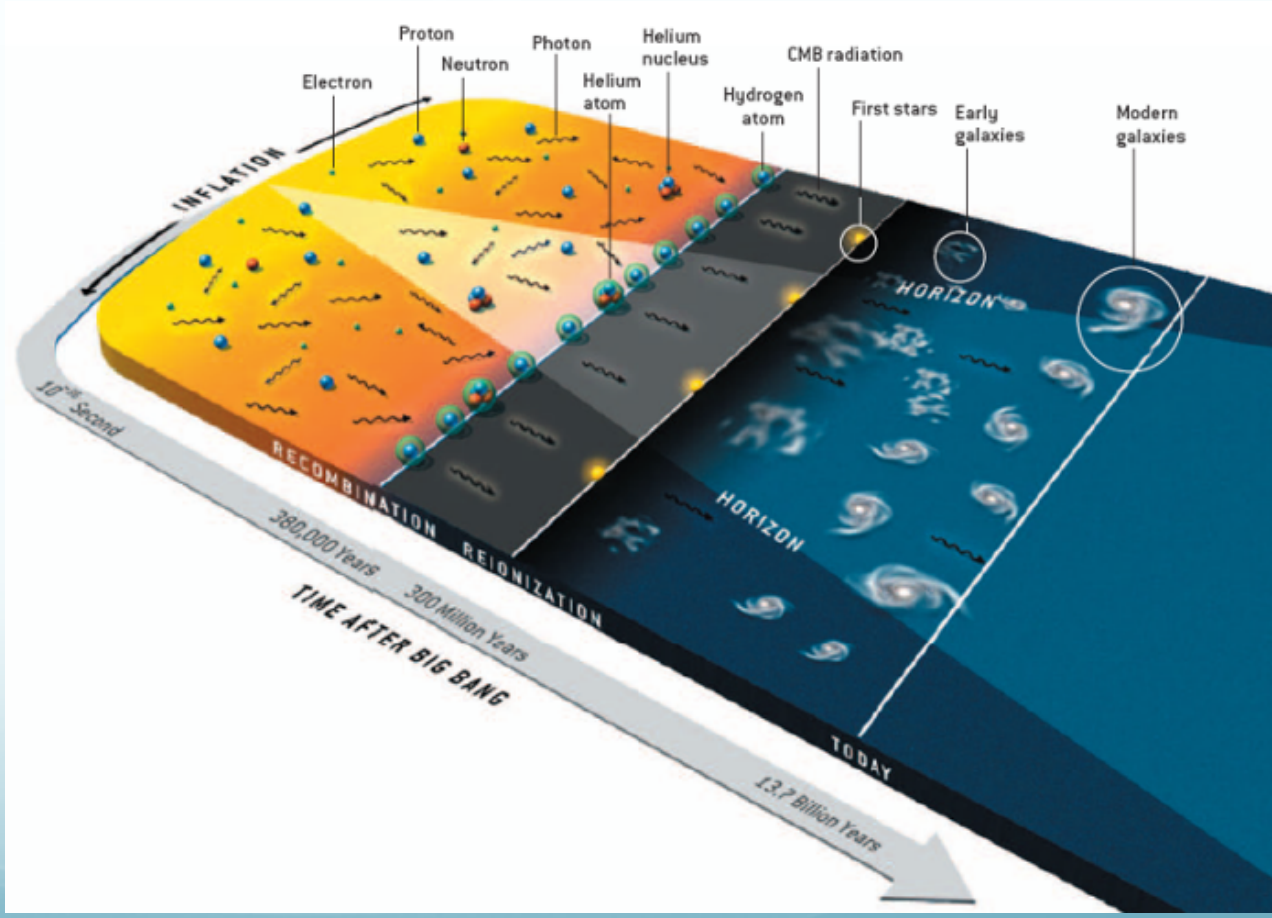

blazars spectra observations:

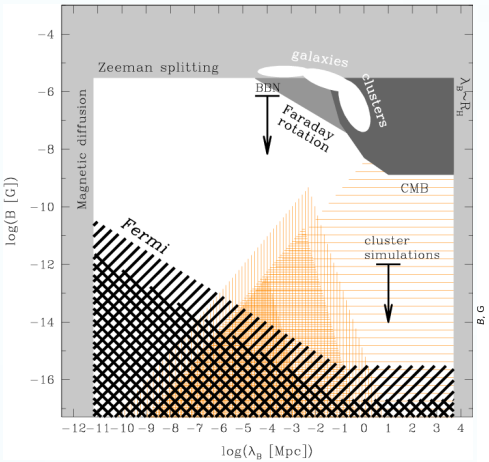

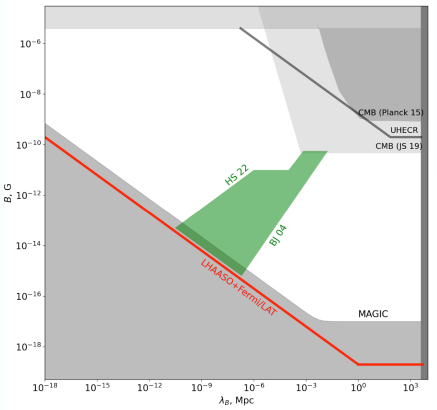

Fig. 2. from Vovk et al. 2024: Lower bound on IGMF derived from the GRB 221009A (red line), compared to existing bounds form γ-ray, radio, CMB and UHECR observations and predictions of the cosmological evolution models. The CMB upper bounds are from Planck (Planck Collaboration et al. 2016) and from the analysis of Jedamzik & Saveliev (2019). UHECR upper bound is from Neronov et al. (2021). MAGIC lower bound is from Acciari et al. (2023). Green-shaded area shows the range of predictions for the endpoints of cosmological evolution of primordial magnetic fields. BJ04 is from Banerjee & Jedamzik (2004), HS22 is from Hosking & Schekochihin (2022).

A. Neronov & E. Vovk,*" Evidence for Strong Extragalactic Magnetic Fields from Fermi Observations of TeV Blazars*", Science 328, 5974 (2010)

E. Vovk, et al.
"Constraint on intergalactic magnetic field from Fermi/LAT observations of the "pair echo" of GRB 221009A" Astron.Astrophys. 683 A25 (2024)

Aharonian, F., et al. (Fermi-LAT, H. E. S. S),
"*Constraints on the intergalactic magnetic field using Fermi-LAT and H.E.S.S. blazar observ*ations". Astrophys. J. Lett. 950, L16 (2023)

V. A. Acciari et al. [MAGIC Collaboration] "*A Lower Bound on Intergalactic Magnetic Fields from Time Variability of 1ES 0229+200 from MAGIC and Fermi/LAT Observations" Astron.Astrophys.* 670 A145 (2023)

S. Archambault et al. [VERITAS Collaboration],
"Search for Magnetically Broadened Cascade Emission From Blazars with VERITAS," Astrophys. J. 835, 288 (2017)

M. Ackermann, et al. [Fermi-LAT Collaboration],
"The Search for Spatial Extension in High-latitude Sources Detected by the Fermi Large Area Telescope," Astrophys. J. Suppl. 237 , 32 (2018)

Primordial or Astrophysical Origin?

E ASTROPHYSICAL JOURNAL LETTERS, 727:L4 (4pp), 2011 January 20 doi:10.1088/2041-8205/727/1/L4

LOWER LIMIT ON THE STRENGTH AND FILLING FACTOR OF EXTRAGALACTIC MAGNETIC FIELDS

K. DOLAG[1,2], M. KACHELRIESS[3], S. OSTAPCHENKO[3,4], AND R. TOMÀS[5]
[1] Universitätssternwarte München, München, Germany
[2] Max-Planck-Institut für Astrophysik, Garching, Germany
[3] Institutt for fysikk, NTNU, Trondheim, Norway
[4] D. V. Skobeltsyn Institute of Nuclear Physics, Moscow State University, Moscow, Russia
[5] II. Institut für Theoretische Physik, Universität Hamburg, Germany
Received 2010 September 16; accepted 2010 November 25; published 2010 December 21

ABSTRACT

High-energy photons from blazars can initiate electromagnetic pair cascades interacting with the extragalactic photon background. The charged component of such cascades is deflected and delayed by extragalactic magnetic fields (EGMFs), thereby reducing the observed point-like flux and potentially leading to multi-degree images in the GeV energy range. We calculate the fluence of 1ES 0229+200 as seen by *Fermi*-LAT for different EGMF profiles using a Monte Carlo simulation for the cascade development. The non-observation of 1ES 0229+200 by *Fermi*-LAT suggests that the EGMF fills at least 60% of space with fields stronger than $\mathcal{O}(10^{-16}$ to $10^{-15})$ G for lifetimes of TeV activity of $\mathcal{O}(10^2$ to $10^4)$ yr. Thus, the (non-)observation of GeV extensions around TeV blazars probes the EGMF in voids and puts strong constraints on the origin of EGMFs: either EGMFs were generated in a space filling manner (e.g., primordially) or EGMFs produced locally (e.g., by galaxies) have to be efficiently transported to fill a significant volume fraction as, e.g., by galactic outflows.

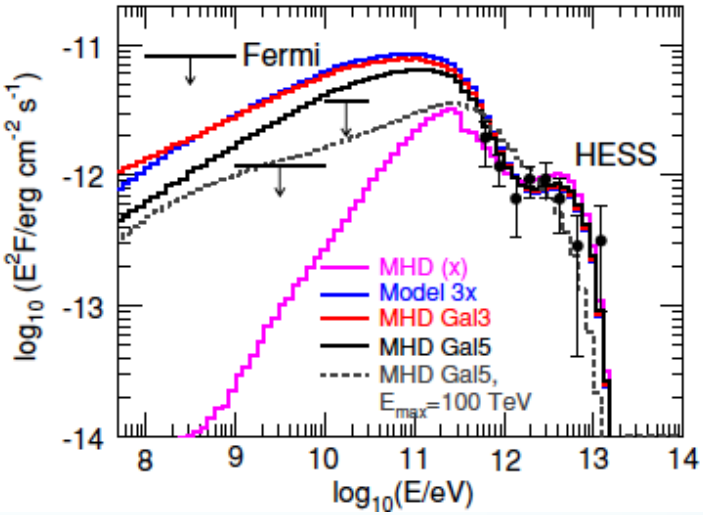

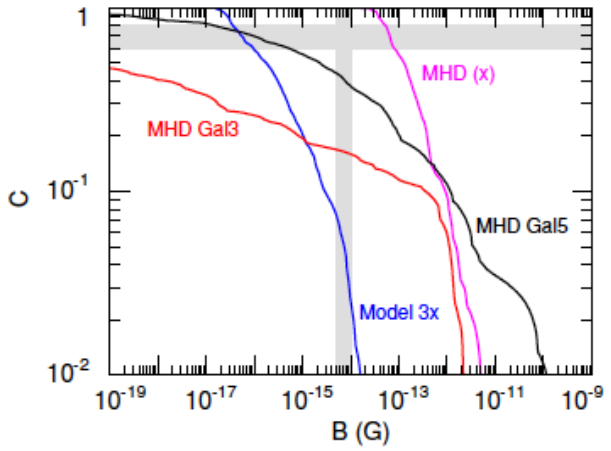

Figure 4. Cumulative volume filling factor $C(B)$ for the four different EGMF models found in MHD simulations.
(A color version of this figure is available in the online journal.)

4. SUMMARY

We have calculated the fluence of 1ES 0229+200 as seen by *Fermi*-LAT using a Monte Carlo simulation for the cascade development. We have discussed the effect of different EGMF profiles on the resulting suppression of the point-like flux seen by *Fermi*-LAT. Since the electron cooling length is much smaller than the mean free path of the TeV photons, a sufficient suppression of the point-like flux requires that the EGMF fills a large fraction along the line of sight toward 1ES 0229+200, $f \gtrsim 0.6$. The lower limit on the magnetic field strength in this volume is $B \sim \mathcal{O}(10^{-15})$ G, assuming 1ES 0229+200 is stable at least for 10^4 yr, weakening by a factor of 10 for $\tau = 10^2$ yr. These limits put very stringent constraints on the origin of EGMFs. Either the seeds for EGMFs have to be produced by a volume filling process (e.g., primordial) or very efficient transport processes have to be present which redistribute magnetic fields that were generated locally (e.g., in galaxies) into filaments and voids with a significant volume filling factor.

testing the early universe

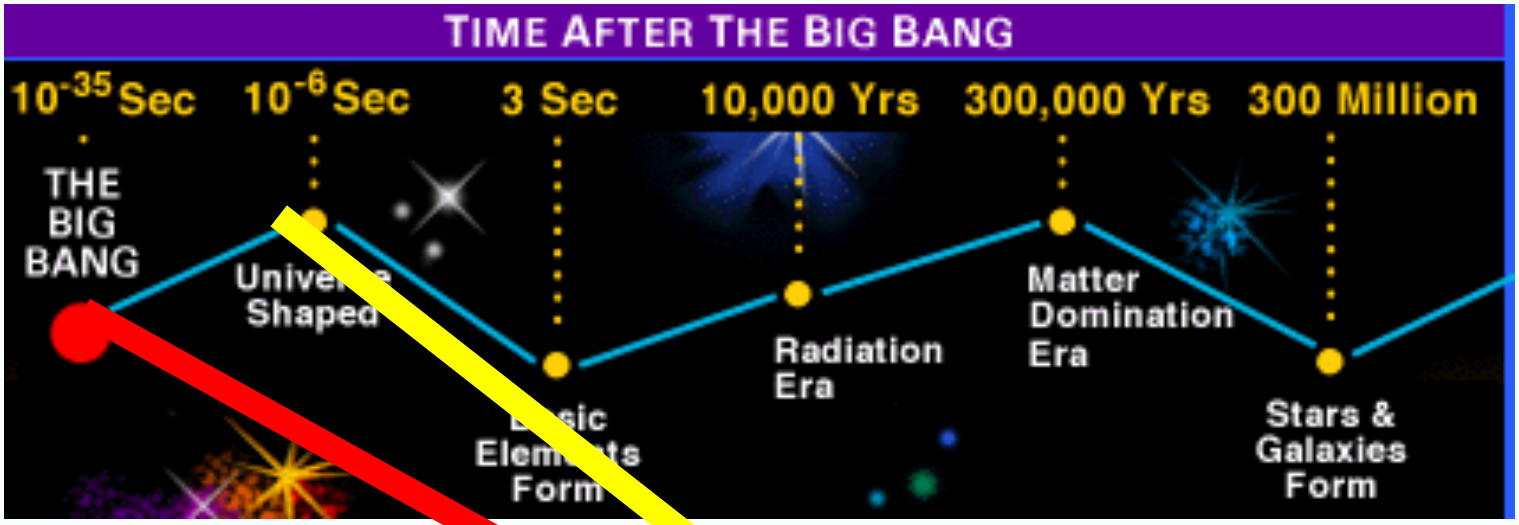

https://visav.phys.uvic.ca/~babul/AstroCourses/P303/BB-slide.htm

magnetic field origin
red-inflation
yellow- phase transitions

https://www.quantamagazine.org/the-hidden-magnetic-universe-begins-to-come-into-view-20200702/

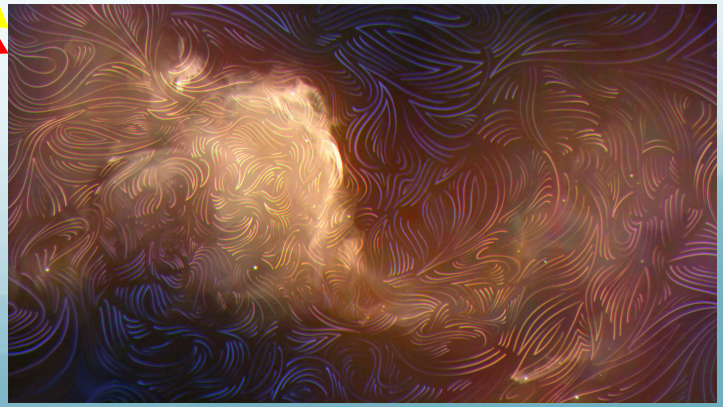

known vs. unknown

What we know

- The amplitude of the magnetic field (galaxies, clusters, voids?)
- The spectral shape of the magnetic field
- The correlation length scale

What we did not know

- When and how magnetic fields were generated
- What new physics is required?
- What were initial conditions

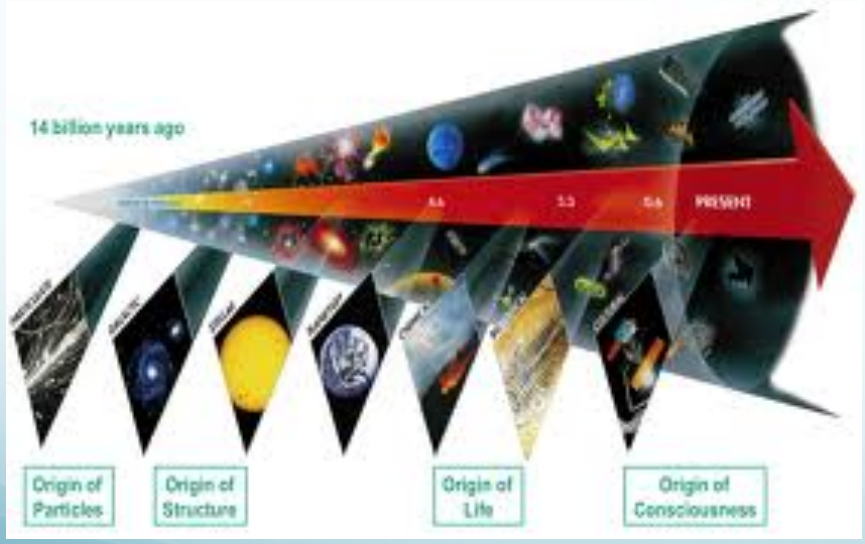

- Acausal
  - ✓ unlimited correlation length
  - ✓ difficulties: backreaction & symmetries violations
- Causal
  - ✓ limited correlation length
  - ✓ difficulties: weak fields

MHD cosmological simulations

Ejection

Primordial

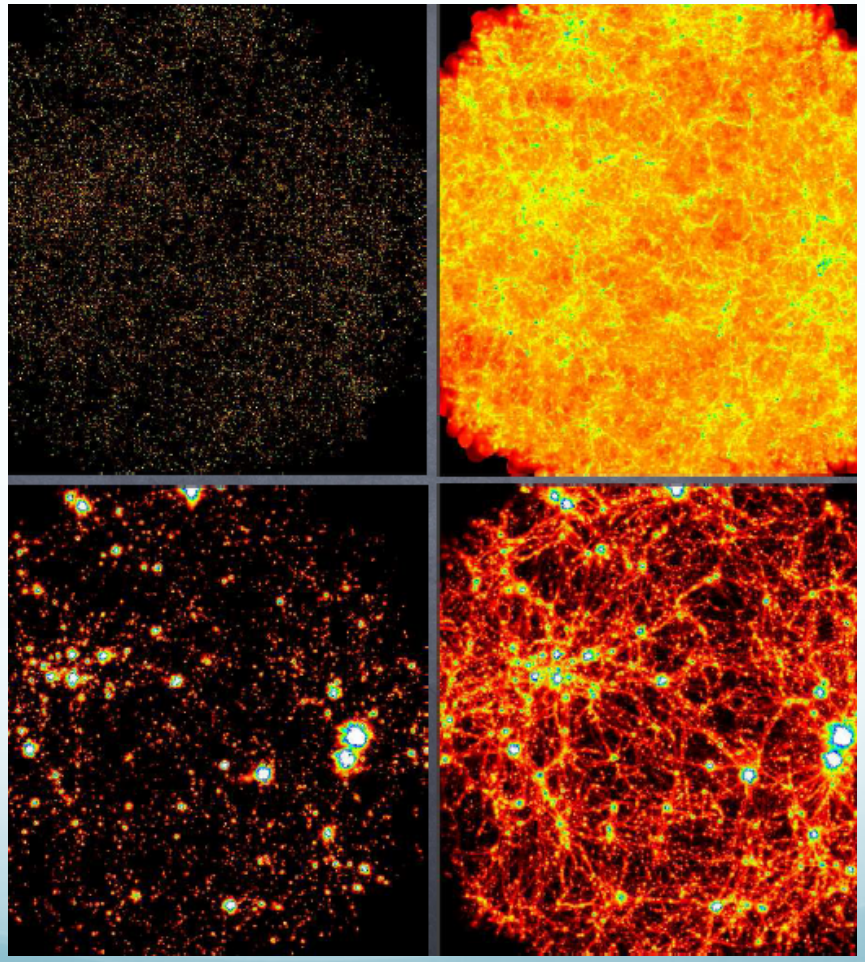

z=4

z=4

z=0

z=0

by *Donnert et al. 2008*

primordial turbulence

- primordial plasma is perfect conductor
- interaction between primordial magnetic fields and fluid (plasma)
- development of turbulence

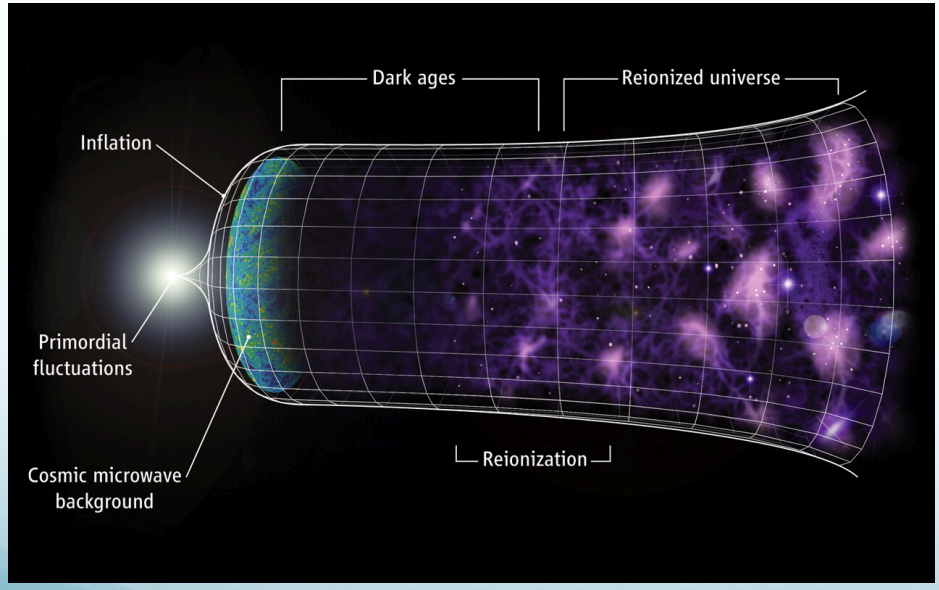

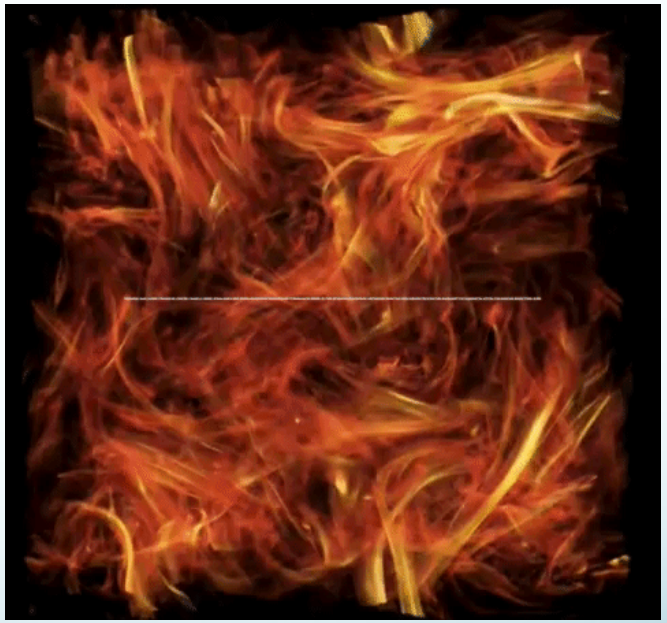

Penders, Jones, Porter, 2019

other sources of primordial turbulence?

Primordial Velocity Fields

- Cosmological Phase Transitions

Bubbles collisions and nucleation

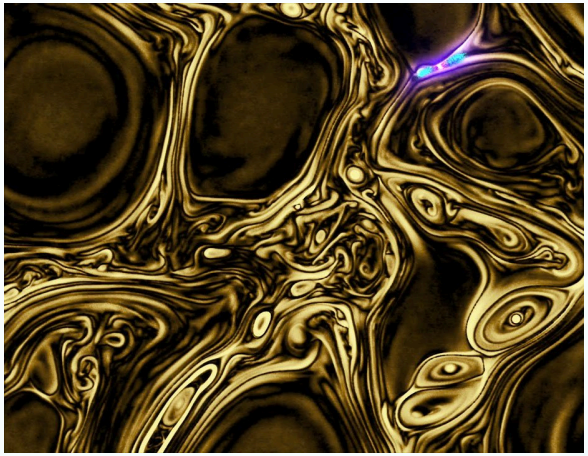

Baym et al. 1995

Quashnock, et al. 1989

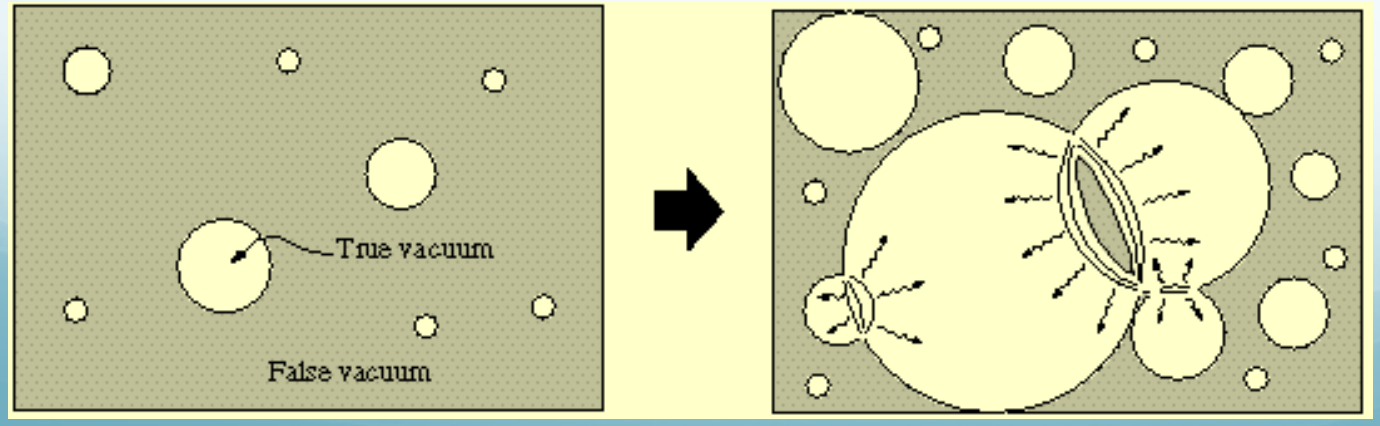

inverse Cauchy problem at work

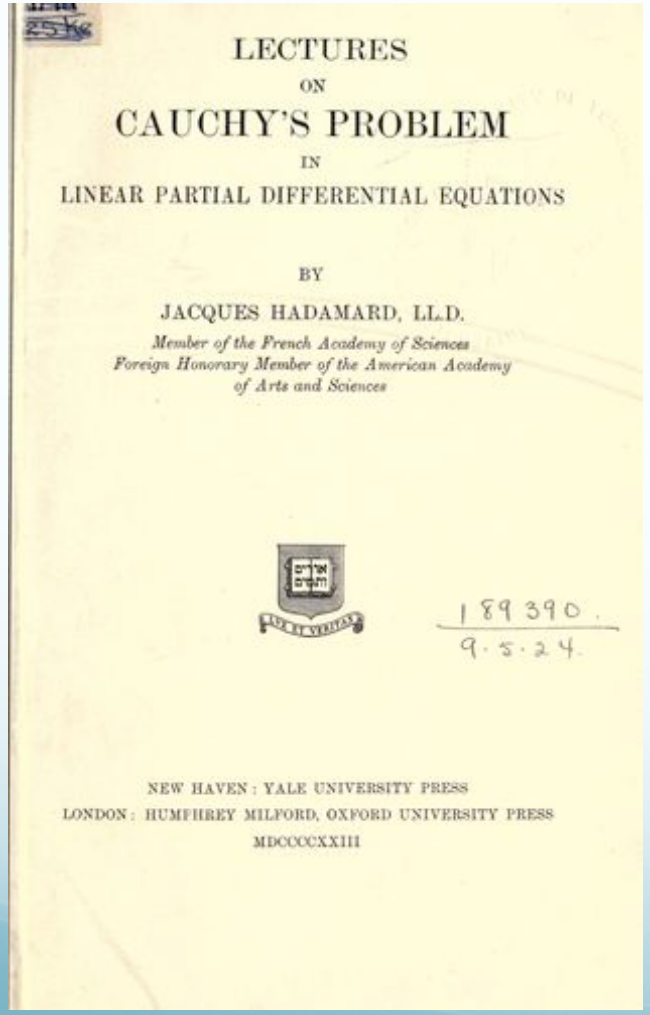

LECTURES
ON
CAUCHY'S PROBLEM
IN
LINEAR PARTIAL DIFFERENTIAL EQUATIONS

BY

JACQUES HADAMARD, LL.D.

Member of the French Academy of Sciences
Foreign Honorary Member of the American Academy of Arts and Sciences

NEW HAVEN: YALE UNIVERSITY PRESS
LONDON: HUMPHREY MILFORD, OXFORD UNIVERSITY PRESS
MDCCCCXXIII

past: input
(initial conditions)

evolution

today: output

Cauchy problem at work - BBN

- Big Bang Nucleosynthesis
  - limits on effective number of relativistic species N_{eff}

$N_{eff}^{(\nu)} = 3.046$ *Salas & Pastor 2016*

+ CMB data $N_{eff} = 2.862 \pm 0.306$ at 95% C.L. *Fields et al. 2019*

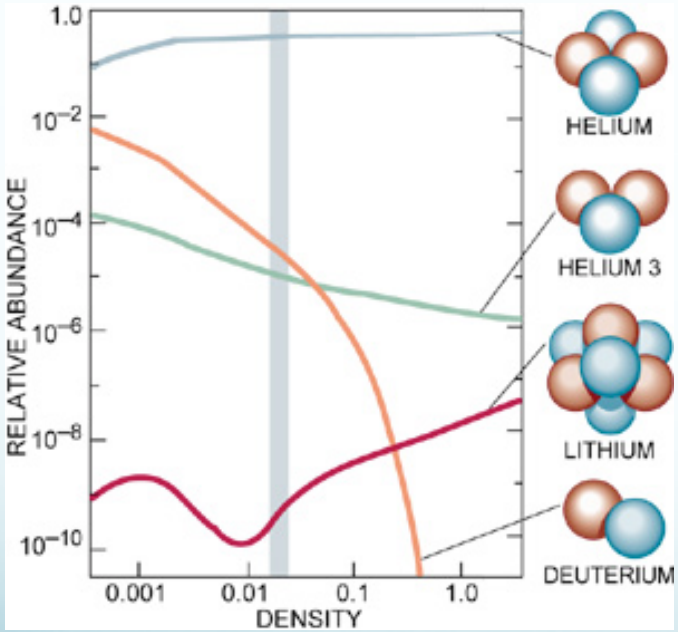

George Gamow

https://w.astro.berkeley.edu/~mwhite/darkmatter/bbn.html

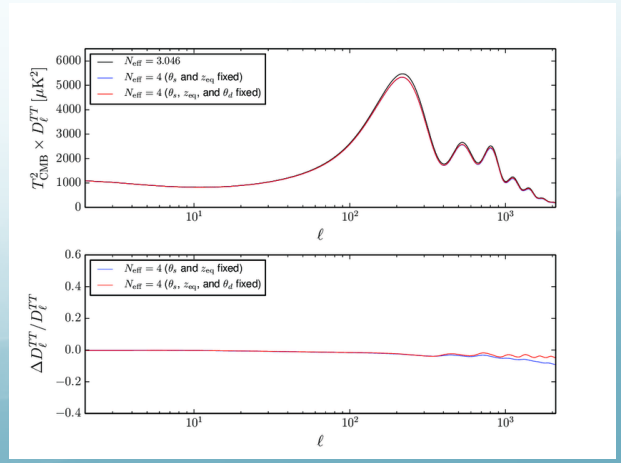

Vagnozzi 2019

BBN & primordial magnetic fields

- **Extra radiation like energy density less than ~3% of the radiation energy density at BBN**

$$\frac{\rho_{\rm add}}{\rho_{\rm rad}} = 0.277\left(\frac{\Delta N_{\rm eff}}{0.122}\right); \qquad \Delta N_{eff} = N_{\rm eff} - N_{\rm eff}^{\nu}$$

- The upper bound on the magnetic (effective) comoving amplitude order of microGauss **at BBN**
- **Limits apply to the total magnetic energy density**

modeling magnetic fields & turbulence

- Homogeneous (statistically) magnetic fields: most of them are related to inflation and the violation of fundamental symmetries such as Lorentz violation (Campanelli et al., 2009) and/or rotational isotropy (Thorne, 1967; Moffatt, 1978; Jacobs, 1969):

$$B_{\rm cr}^{\rm phys} = \frac{mc^2}{e(\hbar/mc)} = 10^{12}\,{\rm G}.$$

Thorne, 1967

- $$B_{\rm com} = B_{\rm phys}\left(\frac{a_*}{a_0}\right) \quad \rightarrow \quad B_{\rm com} \sim 10^{-18}{\rm G}$$

modeling magnetic fields & turbulence

- Statistically isotropic, Gaussian, stochastic magnetic field, $\langle B(\boldsymbol{x})\rangle = 0$: (Monin & Yaglom, v. 2, 1975)

$$\mathcal{B}_{ij}(\mathbf{x},\mathbf{x}+\mathbf{r}) \equiv \langle B_i(\mathbf{x}) B_j(\mathbf{x}+\mathbf{r})\rangle = \mathcal{B}_{ij}(\mathbf{r})$$

$$\mathcal{B}_{ij}(r) = M_N(r)\,\delta_{ij} + [M_L(r) - M_N(r)]\,\hat{r}_i\hat{r}_j + M_H(r)\,\epsilon_{ijl} r_l,$$

$$M_N(r) = \frac{1}{2r}\frac{d}{dr}\left[r^2 M_L(r)\right] = M_L(r) + \frac{r}{2}\frac{d}{dr}M_L(r),$$

$$M_L(r) = \frac{2}{r^2}\int M_N(r) r dr$$

$$\lim_{r\to 0} \mathcal{B}_{ii}(r) = 2\,\mathcal{E}_M$$

$$\int_0^\infty [M_L(r) + 2M_N(r)] r^2 dr = 0,$$

- Divergence free field + finite at infinity $\lim_{r\to\infty} \mathcal{B}_{ii}(r)$ decreases faster than r^{-3}. *Von Karman'1937*.

$$\frac{\mathcal{F}_{ij}(\mathbf{k})}{(2\pi)^3} = P_{ij}(\hat{\mathbf{k}})\frac{E_M(k)}{4\pi k^2} + i\varepsilon_{ijl}\,k_l\,\frac{H_M(k)}{8\pi k^2},$$

$$\mathcal{E}_M = \int_0^\infty dk\, E_M(k), \qquad \mathcal{H}_M = \int_0^\infty dk\, H_M(k).$$

$$\xi_M = \frac{1}{\mathcal{E}_M}\int_0^\infty dk\, k^{-1}\, E_M(k), \qquad |\mathcal{H}_M| \leq 2\xi_M \mathcal{E}_M;$$

$$4\pi k^2 \mathcal{F}_{NN} = E_M(k) \;\rightarrow \lim_{k\to 0} E_M(k) = k^4$$

True for same time correlations

$$\lambda = \left\{ -\frac{B(0)}{2B''(0)} \right\}^{1/2} =$$

$$= \left\{ \frac{3\int_0^\infty E(k)\,dk}{2\int_0^\infty k^2 E(k)\,dk} \right\}^{1/2}.$$

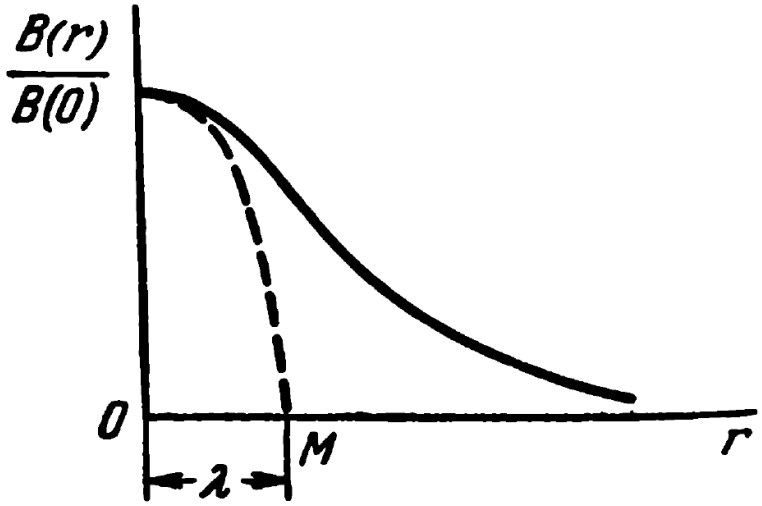

FIG. 4 Definition of the length scale λ.

$$\bar{\varepsilon} = 2\nu \int_0^\infty k^2 E(k)\,dk =$$

time dependent processes

conservation laws – invariants – symmetries

- **Noether's theorem:** every continuous symmetry of the action of a physical of a physical system with conservatives forces has a corresponding conservation law.
- it does not apply to systems that cannot be modeled with a Lagrangian alone. In particular, dissipative systems with continuous symmetries need not have a corresponding conservation law.

dissipation – Kolmogorov spectrum

$$E(k) \equiv \frac{1}{w}\frac{d\rho_{\rm turb}}{dk} = C_k \bar{\varepsilon}^{2/3} k^{-5/3},$$

$$\bar{\varepsilon} = 2\nu \int_{k_S}^{k_D} dk\, k^2 E(k)$$

$$u_L \simeq \left[\int_{k_L}^{k_D} dk\, E(k)\right]^{1/2} = \left(\frac{3}{2}\right)^{1/2} (2\pi)^{-1/3} (\bar{\varepsilon} L)^{1/3}.$$

We can also estimate an eddy turnover time scale (known as the circulation time) on a length scale L as the ratio of L to the physical velocity $v_L = u_L/(1+u_L^2)^{1/2}$. We argue below that the physical velocity will be approximately bounded by the sound speed of the fluid; for a radiation-dominated plasma, this condition is $v_L \le 1/\sqrt{3}$. Making the simple approximation that $v_L = u_L$ until the sound speed is reached, after which time v_L is the sound speed, the circulation time is

$$\tau_L \simeq L/v_L \simeq \begin{cases} \frac{3}{2}\bar{\varepsilon}^{-1/3} L^{2/3}, & L \le 3^{3/2}(8\bar{\varepsilon})^{-1}; \\ L\sqrt{3}, & \text{otherwise.} \end{cases} \qquad (12)$$

Kosowsky, Mack, TK, 2002

Loitsiansky invariant

$$B_{ij}(r,\ t) = [B_{LL}(r,\ t) - B_{NN}(r,\ t)]\ \frac{r_i r_j}{r^2} + B_{NN}(r,\ t)\delta_{ij},$$

$$B_{LL}(r,\ t) = \overline{u_L(x,\ t)\, u_L(x+r,\ t)},\quad B_{NN}(r,\ t) = \overline{u_N(x,\ t)\, u_N(x+r,\ t)}$$

$$B_{ij,\ k}(r,\ t) = \overline{u_i(x,\ t)\, u_j(x,\ t)\, u_k(x+r,\ t)}$$

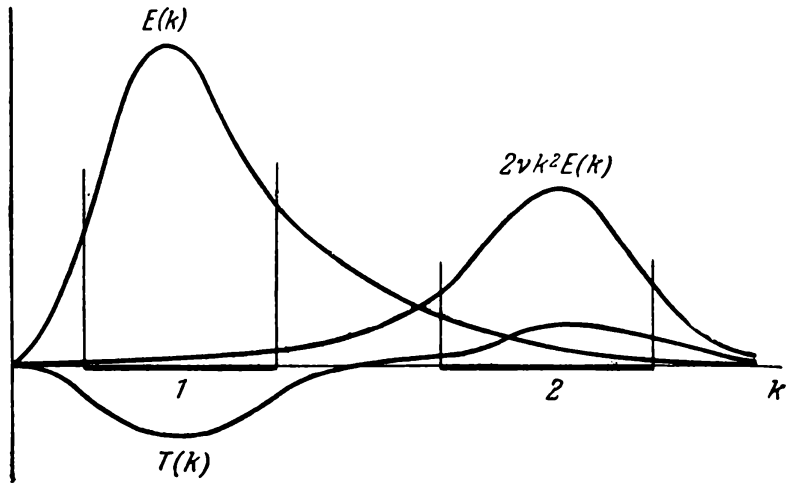

FIG. 12 Schematic illustration of the energy spectrum $E(k)$, the energy dissipation spectrum $2\nu k^2 E(k)$, and the function $T(K)$. 1) Energy range; 2) dissipation range.

$$\frac{\partial F_{ij}(k,\ t)}{\partial t} = -\,2\nu k^2 F_{ij}(k,\ t).$$

$$F(k,\ t) = F(k,\ t_0)\, e^{-2\nu k^2 (t - t_0)},$$

$$v^2(t) \sim (t - t_0)^{-10/7},\quad l(t) \sim (t - t_0)^{2/7}$$

Corsin Invariants

$$\lim_{V\to\infty}\frac{1}{V}\overline{\left[\int_V \rho'(x)\,dx\right]^2} = 4\pi\Lambda_1 = \text{const},$$

$$\lim_{V\to\infty}\frac{1}{V}\overline{\left[\int_V u(x)\,dx\right]^2} = 4\pi\Lambda_2 = \text{const},$$

$$\lim_{V\to\infty}\frac{1}{V}\overline{\left[\int_V g'(x)\,dx\right]^2} = 4\pi\Lambda_3 = \text{const},$$

$$\lim_{V\to\infty}\frac{1}{V}\overline{\int_V \rho'(x)\,dx\int_V g'(x)\,dx} = 4\pi\Lambda_4 = \text{const},$$

sound waves from turbulence

Aeroacoustic: Sound waves generation by turbulence

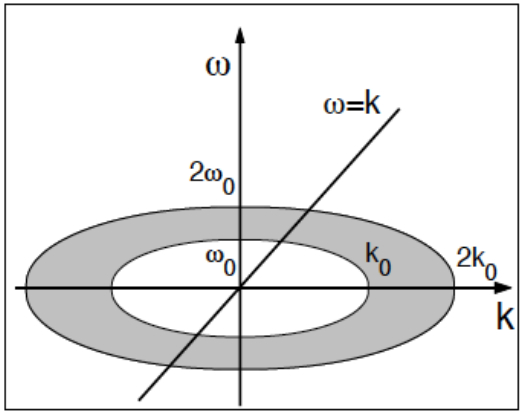

FIG. 1: To the determination of the characteristic frequency of the GWs generated by turbulence. Dark area contains main part of turbulent energy.

$$\left(\frac{\partial^2}{\partial t^2} - c_s^2 \nabla^2\right) \rho' = \frac{\partial^2 T_{ij}}{\partial x_i \partial x_j},$$

Lighthill, 1952
Proudman 1952

$$\frac{\partial^2 P}{\partial t^2} - a_0^2 \Delta P = - \frac{\partial^2 T_{ij}}{\partial x_i \partial x_j}, \tag{20.25}$$

where

$$T_{ij}(x, t) = u_i^{(s)}(x, t)\, u_j^{(s)}(x, t), \tag{20.26}$$

[$u^{(s)}(x, t)$ is the incompressible component of the velocity field], and, as above, $P = p/\gamma\bar{p}$, $a_0^2 = \gamma\bar{p}/\bar{\rho}$. We recall that when we derived this equation we neglected viscosity and thermal conductivity effects, while the density fluctuations $\rho' = \rho - \bar{\rho}$ were assumed to be small in comparison with $\bar{\rho}$ (which implied that the velocity divergence was also small). Moreover, typical values of the incompressible velocity fluctuations $u^{(s)}$ were assumed to be small in comparison with the mean sound velocity a_0. Equation (20.25) can therefore be regarded as describing the generation of sound by arbitrary turbulence with small Mach number $\mathrm{Ma} = U/a_0$, and not merely by a turbulence approaching the final period of decay.[40] In the limit as $a_0 \to \infty$, Eq. (20.25) becomes identical with Eq. (1.9), i.e., with the usual equation relating the velocity and pressure fields in an incompressible fluid.

Equation (20.25) leads to a number of important consequences. For example, the right-hand side of this equation is a combination of the second derivatives of the field $T_{ij}(x)$ (namely, the divergence of this field with respect to both its indices), which means that, in the absence of solid walls, the generation of sound waves by the turbulence is equivalent to radiation by a set of acoustic quadrupoles (and not the usual sound sources or dipole sources), This fact was pointed out by Lighthill (1952, 1954). Hence it follows that, if there are no walls, a low Mach number turbulence is not an effective source of sound. This is also supported by the character of the dependence of the total intensity of the radiated acoustic waves on the characteristic velocity scale U. The general solution of Eq. (20.25) can be written in terms of the retarded potentials:

$$P'(x, t) = P(x, t) - \bar{P} = \frac{1}{4\pi a_0^2} \int \left. \frac{\partial^2 T_{ij}(y, \tau)}{\partial y_i \partial y_j} \right|_{\tau = t - \frac{|x-y|}{a_0}} \frac{dy}{|x-y|}. \tag{20.27}$$

We shall suppose that acoustic "noise" is generated by a bounded volume of the fluid in which there are velocity fluctuations, while the surrounding medium is at rest. In that case, the "turbulent region" will emit acoustic waves in all directions, giving rise to the pressure fluctuations described by Eq. (20.27) outside this region. If we apply the integral Gauss formula twice to the right-hand side of Eq. (20.27), and bear in mind that the integrals over the bounding surface, which lies outside the turbulence region, are identically equal to zero, we can replace differentiation with respect to the running coordinates y_l in Eq. (20.27) by differentiation of the integrand with respect to the coordinates of the point of observation $\boldsymbol{x}$:

$$P'(\boldsymbol{x}, t) = \frac{1}{4\pi a_0^2} \frac{\partial^2}{\partial x_i \, \partial x_j} \int T_{ij}\left(\boldsymbol{y}, t - \frac{|\boldsymbol{x}-\boldsymbol{y}|}{a_0}\right) \frac{d\boldsymbol{y}}{|\boldsymbol{x}-\boldsymbol{y}|} \qquad (20.28)$$

[We note that the appearance of the second derivative of the integral on the right-hand side of Eq. (20.28) corresponds to the fact that the radiation is a quadrupole radiation]. Let us consider the field $P(\boldsymbol{x}, t)$, well away from the "noisy" volume, i.e., at a distance much greater than the characteristic wavelength of the emitted sound. This will be the so-called wave-zone approximation. The leading contribution to the right-hand side of Eq. (20.28) will then be due to terms obtained by differentiating the tensor $T_{ij}\left(\boldsymbol{y}, t - \frac{|\boldsymbol{x}-\boldsymbol{y}|}{a_0}\right)$ with respect to x_i and x_j, and consequently

$$P'(\boldsymbol{x}, t) \approx \frac{1}{4\pi a_0^4} \int \frac{r_i r_j}{r^3} \frac{\partial^2}{\partial \tau^2} T_{ij}(\boldsymbol{y}, \tau)\Big|_{\tau = t - \frac{r}{a_0}} d\boldsymbol{y}, \quad r = |\boldsymbol{x}-\boldsymbol{y}|. \qquad (20.29)$$

Since, for Mach numbers much less than unity, the tensor T_{ij} is proportional to the square of the turbulent velocity fluctuations, and the velocity $u^{(s)}$ can be assumed to be equal to the total velocity fluctuation u, we see that the amplitude of the pressure fluctuation in the wave zone is proportional to the square of the characteristic value U of the velocity fluctuations, multiplied by the square of the characteristic frequency. However, the characteristic fluctuation frequency is proportional to U/L, where L is the turbulence length scale. The amplitude of the pressure fluctuations is therefore proportional to U^2, and the total emitted energy (intensity of the sound waves) is proportional to U^8. This means that the emitted sound intensity will be very low when the velocity U is low.

The above result can be made more precise as follows. It is readily shown that the energy flux density carried by the sound waves in the wave zone is given by

$$j_E = \frac{a_0^3 \overline{\rho'^2}}{\bar{\rho}} = a_0^3 \bar{\rho} \overline{P'^2} \tag{20.30}$$

[see, for example, Landau and Lifshits (1953), Sect. 64]. In the wave zone, i.e., at distances from the "turbulent volume" that are much greater than the linear dimensions D of the volume, the factor $r_i r_j / r^3$ in Eq. (20.29) can be regarded as constant and taken outside the integral sign. Hence in this zone the energy carried by the sound waves is given by

$$j_E(x) = \frac{\bar{\rho}}{16\pi^2 a_0^4} \frac{r_i r_j r_k r_l}{r^6} \times$$

$$\times \int\int \overline{\frac{\partial^2}{\partial \tau^2} [u_i(y, \tau) u_j(y, \tau)]_{\tau = t - \frac{|x-y|}{a_0}} \frac{\partial^2}{\partial \tau'^2} [u_k(y', \tau') u_l(y', \tau')]_{\tau' = t - \frac{|x-y'|}{a_0}}} \times$$

$$\times dy\, dy'. \tag{20.31}$$

It is readily seen that we can neglect in this formula the difference between τ and τ'. In fact, since the correlation between the tensors $T_{ij}(y, \tau)$ and $T_{kl}(y', \tau')$ is appreciable only for $|y - y'| < L$, we have $|\tau - \tau'| \lesssim \frac{L}{a_0} = \frac{L}{U}\frac{U}{a_0}$ and, consequently, for $\mathrm{Ma} = \frac{U}{a_0} \ll 1$ the difference $\tau - \tau'$ will be much less than the time scale L/U of the turbulence fluctuations. The mean value under the integral sign in Eq. (20.31) can therefore be evaluated on the assumption that $\tau = \tau'$. The integral with respect to y' in Eq. (20.31) can then be roughly estimated by assuming that for any fixed y, it is equal to the quantity

$$\overline{\frac{\partial^2 u_l(y, \tau)\, u_j(y, \tau)}{\partial \tau^2}\, \frac{\partial^2 u_k(y, \tau)\, u_l(y, \tau)}{\partial \tau^2}},$$

which is of the order of

$$U^4 \left(\frac{U}{L}\right)^4 = \frac{U^8}{L^4}$$

multiplied by the characteristic volume L^3 of the fluid in which the velocity fluctuations are appreciably correlated with the velocity fluctuations at the given point y. This shows that the total energy $\mathcal{E}$ emitted per unit time by a unit mass of the turbulent medium is of the order of

$$\mathcal{E} \sim U^8 / a_0^5 L \tag{20.32}$$

[since the quantity $\mathcal{E}$ is equal to the integral of the right-hand side of Eq. (20.31) evaluated over a sphere of radius r, divided by $\overline{\rho}$ and the total volume of the turbulent region]. If we recall that the rate of turbulent-energy dissipation is of the order of U^3/L (see Sect. 16.5), we can rewrite Eq. (20.32) in the form

$$\mathcal{E} \sim \bar{\varepsilon} \frac{U^5}{a_0^5} = \bar{\varepsilon}\, (\mathrm{Ma})^5. \tag{20.33}$$

gravitational waves primordial turbulence?

$$\nabla^2 \delta\rho(\boldsymbol{x},t) - \frac{1}{c_s^2}\frac{\partial^2}{\partial t^2}\delta\rho(\boldsymbol{x},t) = -\frac{\partial^2}{\partial x^i \partial x^j} T(\boldsymbol{x},t), \qquad c_s^2 = \frac{\partial p}{\partial \rho}$$

$$\nabla^2 h_{ij}(\boldsymbol{x},t) - \frac{\partial^2}{\partial t^2} h_{ij}(\boldsymbol{x},t) = -16\pi G\, S_{ij}(\boldsymbol{x},t) \qquad c = 1$$

Aero-acoustic approximation:

- ✓ sound waves generation by turbulence
- ✓ gravitational waves generation

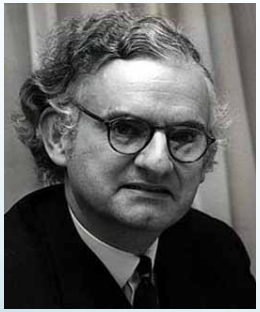

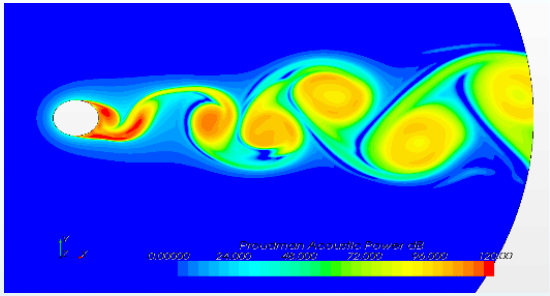

Lighthill, 1952; Proudman 1952

Kosowsky, Mack, Kahniashvili, 2002
Dolgov, Grasso, Nicolis, 2002

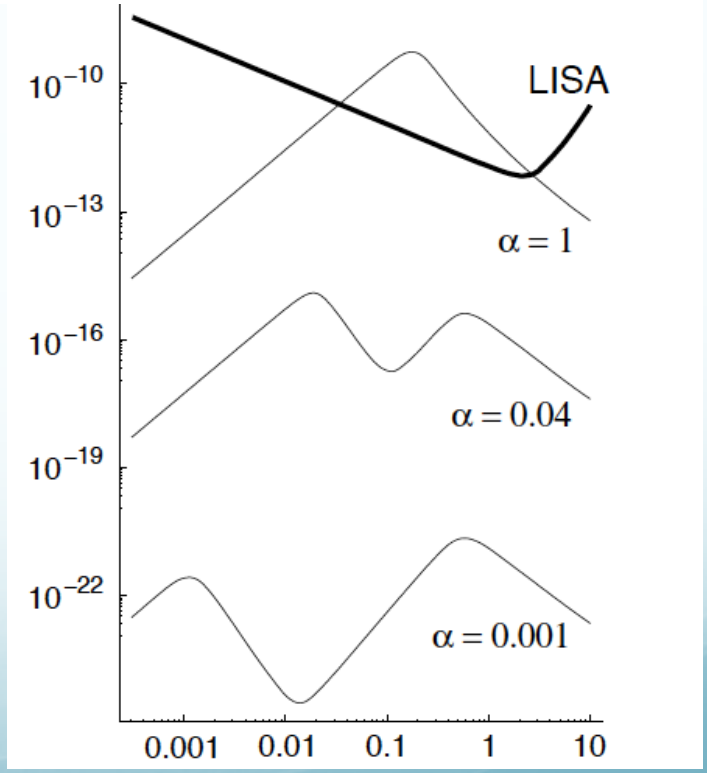

Nicolis 2004

aeroacoustic approximation

Gogoberidze, TK, Kosowsky, 2007

$$\nabla^2 h_{ij}(\mathbf{x},t) - \frac{\partial^2}{\partial t^2} h_{ij}(\mathbf{x},t) = -16\pi G S_{ij}(\mathbf{x},t).$$

$$h_{ij}(\mathbf{x},t) = 4G \int \mathrm{d}^3\mathbf{x}' \frac{S_{ij}(\mathbf{x}', t - |\mathbf{x}-\mathbf{x}'|)}{|\mathbf{x}-\mathbf{x}'|}.$$

$$\rho_{GW}(\mathbf{x},t) = \frac{1}{32\pi G}\langle \partial_t h_{ij}(\mathbf{x},t)\partial_t h_{ij}(\mathbf{x},t)\rangle = \frac{G}{2\pi}\int \mathrm{d}^3\mathbf{x}'\mathrm{d}^3\mathbf{x}'' \frac{\langle \partial_t S_{ij}(\mathbf{x}',t')\partial_t S_{ij}(\mathbf{x}'',t'')\rangle}{|\mathbf{x}-\mathbf{x}'||\mathbf{x}-\mathbf{x}''|},$$

$$\mathbf{P}(\mathbf{x}) = \frac{G\hat{\mathbf{n}}}{2\pi|\mathbf{x}|^2}\int \mathrm{d}^3\mathbf{x}'\mathrm{d}^3\mathbf{x}''\langle \partial_t S_{ij}(\mathbf{x}',t')\partial_t S_{ij}(\mathbf{x}'',t'')\rangle.$$

$$L(\mathbf{x},\tau) \equiv \frac{1}{32\pi G}\langle \partial_t h_{ij}(\mathbf{x},t)\partial_t h_{ij}(\mathbf{x},t+\tau)\rangle,$$

For the case of stationary turbulence, it can be proven that [23]

$$\langle \partial_t S_{ij}(\mathbf{x}', t')\partial_t S_{ij}(\mathbf{x}'', t'')\rangle = -\partial_\tau^2 \langle S_{ij}(\mathbf{x}', t')S_{ij}(\mathbf{x}'', t'')\rangle. \tag{12}$$

Using Eq. (12) with the far-field approximation $|\mathbf{x}-\mathbf{x}'| = |\mathbf{x}| - \mathbf{x}\cdot\mathbf{x}'/|\mathbf{x}|$, and using the fact that the cross-correlation of a stationary random function is independent of time translation, Eq. (11) reduces to

$$L(\mathbf{x}, \tau) = \frac{-G}{2\pi|\mathbf{x}|^2}\partial_\tau^2 \int \mathrm{d}^3\mathbf{x}'\mathrm{d}^3\mathbf{x}''\langle S_{ij}(\mathbf{x}', t)S_{ij}(\mathbf{x}'', \tau')\rangle, \tag{13}$$

where

$$\tau' = t + \tau + \frac{\mathbf{x}}{|\mathbf{x}|}\cdot(\mathbf{x}'' - \mathbf{x}'). \tag{14}$$

Defining the two-point time-delayed forth order correlation tensor by

$$R_{ijkl}(\mathbf{x}', \boldsymbol{\xi}, \tau) = \frac{1}{\mathrm{w}^2}\langle S_{ij}(\mathbf{x}', t)S_{kl}(\mathbf{x}'', t+\tau)\rangle, \tag{15}$$

where $\boldsymbol{\xi} = \mathbf{x}'' - \mathbf{x}'$ and $\mathrm{w} = \rho + p$ is the enthalpy density of the plasma, Eq. (13) yields

$$L(\mathbf{x}, \tau) = \frac{-G\mathrm{w}^2}{2\pi|\mathbf{x}|^2}\partial_\tau^2 \int \mathrm{d}^3\mathbf{x}'\mathrm{d}^3\xi R_{ijij}\left(\mathbf{x}', \boldsymbol{\xi}, \tau + \frac{\mathbf{x}}{|\mathbf{x}|}\cdot\xi\right). \tag{16}$$

Fourier transforming this equation gives

$$I(\mathbf{x}, \omega) = \frac{4\pi^2\omega^2 G\mathrm{w}^2}{|\mathbf{x}|^2}\int \mathrm{d}^3\mathbf{x}' H_{ijij}\left(\mathbf{x}', \frac{\mathbf{x}}{|\mathbf{x}|}\omega, \omega\right) \tag{17}$$

$$\rho_{GW}(\omega) \equiv \frac{d\rho_{GW}}{d\,\ln\omega} = 16\pi^3\omega^3 G\mathrm{w}^2\tau_T H_{ijij}(\omega, \omega).$$

We assume that the stirring and dissipation scales are well separated, i.e., $k_0 \ll k_d$, which corresponds to the turbulence having high Reynolds number. This will be an excellent approximation in any early universe phase transition with the stirring scale related to the Hubble length. For simplicity, we adopt Kraichnan's square exponential time dependence [34] to model the temporal decorrelation,

$$f(\eta_k, \tau) = \exp\left(-\frac{\pi}{4}\eta_k^2\tau^2\right). \tag{26}$$

While other forms of $f(\eta_k, \tau)$ are also frequently used (see, e.g., [37]), neither total power of generated waves nor the spectrum are very sensitive to the specific form of the temporal decorrelation [21].

$$F_{ij}(\mathbf{k}, \tau) = \frac{E_k}{4\pi k^2}\left(\delta_{ij} - \frac{k_i k_j}{k^2}\right) f(\eta_k, \tau),$$

$$E_k = C_K \varepsilon^{2/3} k^{-5/3}, \qquad k_0 < k < k_d,$$

$$\eta_k = \frac{1}{\sqrt{2\pi}}\varepsilon^{1/3} k^{2/3}.$$

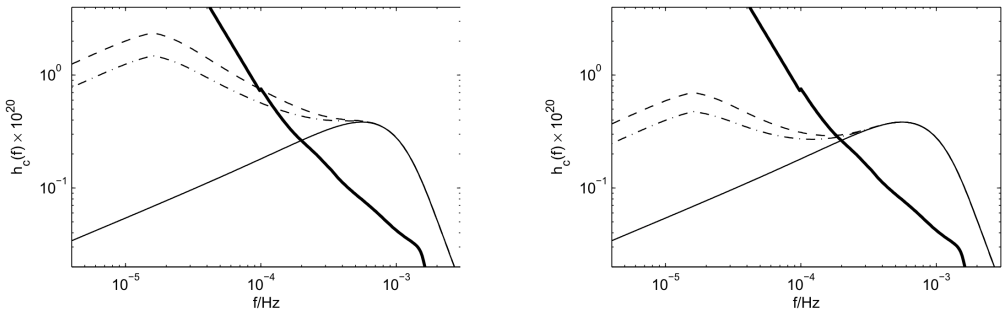

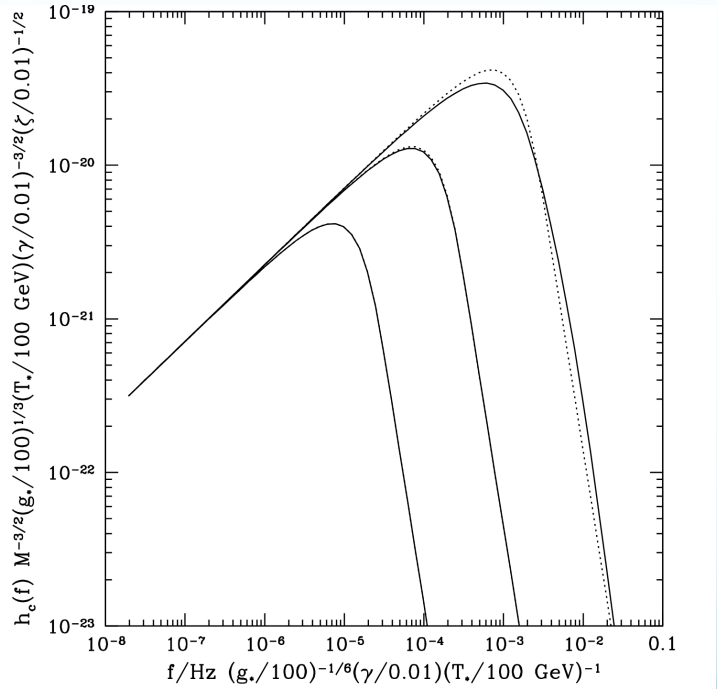

FIG. 1: The spectrum of the gravitational wave strain amplitude, $h_C(f)$, as a function of the frequency f for a first-order phase transition with $g_* = 100$, $T_* = 100$ GeV, $\alpha = 0.5$, and $\beta = 100H_\star$, from hydrodynamic Kolmogorov turbulence with zero magnetic helicity (solid lines) and for the two MHD turbulence models, Model A (dash-dotted lines) and Model B (dashed lines). The left panel corresponds to initial magnetic helicity $\zeta_\star = 0.15$, while $\zeta_\star = 0.05$ in the right panel. In both panels the bold solid line corresponds to the 1-year, 5σ LISA design sensitivity curve [48] including confusion noise from white dwarf binaries [49].

Numerical Simulations

- To account properly non-linear processes (MHD)
- Not be limited by the short duration of the phase transitions
- Two stages turbulence decay
  - Forced turbulence
  - Free decay
- The source is present till recombination (after the field is frozen in)
- Results – strongly initial conditions dependent

$$\left(\frac{\partial^2}{\partial t^2} - c^2\nabla^2\right) h_{ij}^{\mathrm{TT}} = \frac{16\pi G}{a^3 c^2} T_{ij}^{\mathrm{TT}},$$

Grishchuk 1974

$$h_{ij}^{\mathrm{TT}} = a h_{ij}^{\mathrm{TT,phys}}$$

$$\mathrm{d}t_{\mathrm{phys}} = a\mathrm{d}t$$

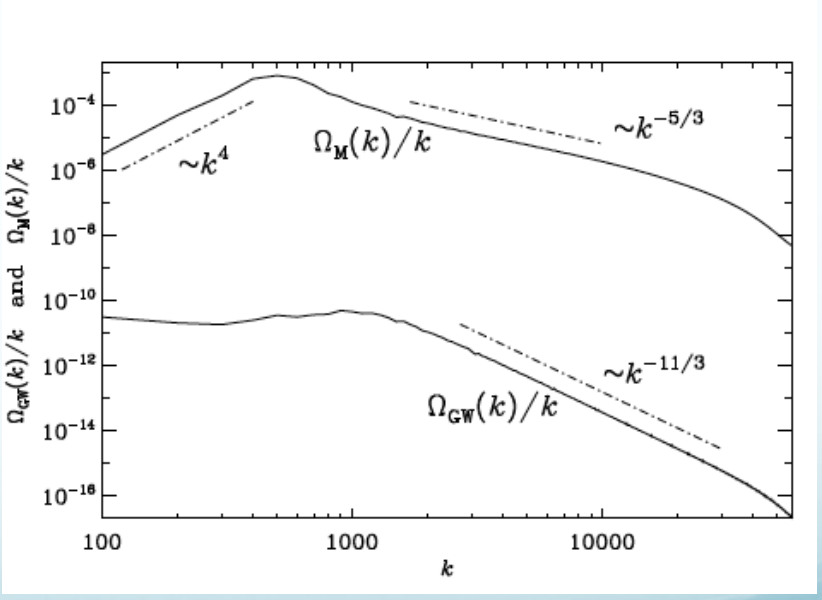

Magnetic and GW energy spectra averaged over late times ($t > 1.1$), after the GW spectrum has started to fluctuate around a steady state.

Roper Pol et al. 2019

Why Numerical Modeling Is Necessary

- ✓ It is assumed the stationary turbulence while in reality turbulence decays

$$\mathcal{E}_M(t) \simeq \mathrm{w} b_1^2 \left(1 + \frac{t}{\tau_1}\right)^{-2/3},$$

$$\mathcal{E}_v(t) \simeq \mathrm{w} v_1^2 \left(1 + \frac{t}{\tau_1}\right)^{-2/3},$$

- ✓ Three stages of generation

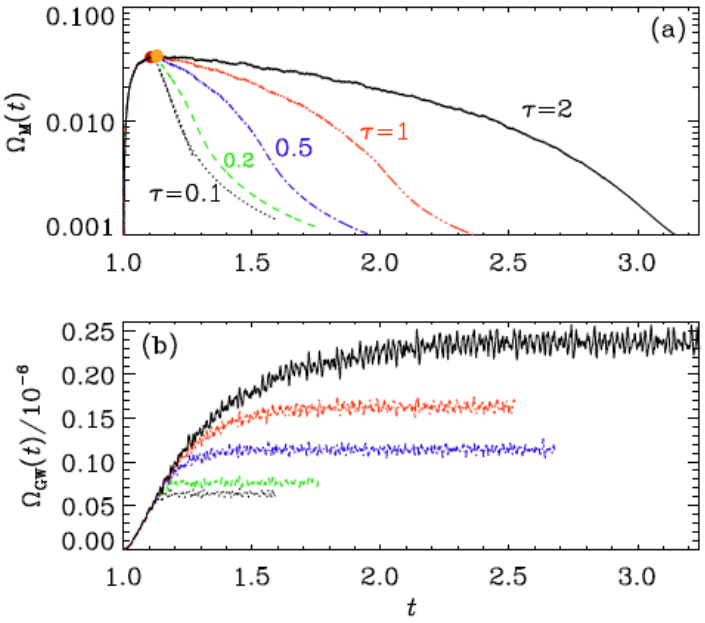

FIG. 1: Evolution of magnetic energy (top) and growth of GW energy density (bottom) for simulations where the driving is turned off at $t = 1.1$ (black dotted line), or the strength of the driving is reduced linearly in time over the duration $\tau = 0.2$ (green), 0.5 (blue), 1 (red), or 2 (black). Time is in units of the Hubble time at the moment of source activation.

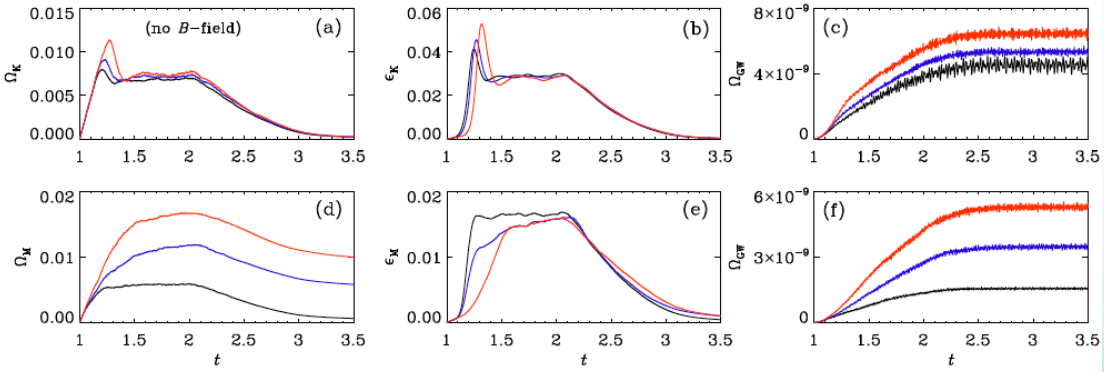

FIG. 2: Evolution of (a) Ω_K, (b) ϵ_K, and (c) Ω_{GW} for kinetically driven cases with $\sigma = 0$ (black), 0.5 (blue), and 1 (red), and of (d) Ω_M, (e) ϵ_M, and (f) Ω_{GW} for magnetically driven cases with $\sigma = 0$ (black), 0.3 (blue), and 1 (red).

Kahniashvili et al. 2020

describing primordial turbulence

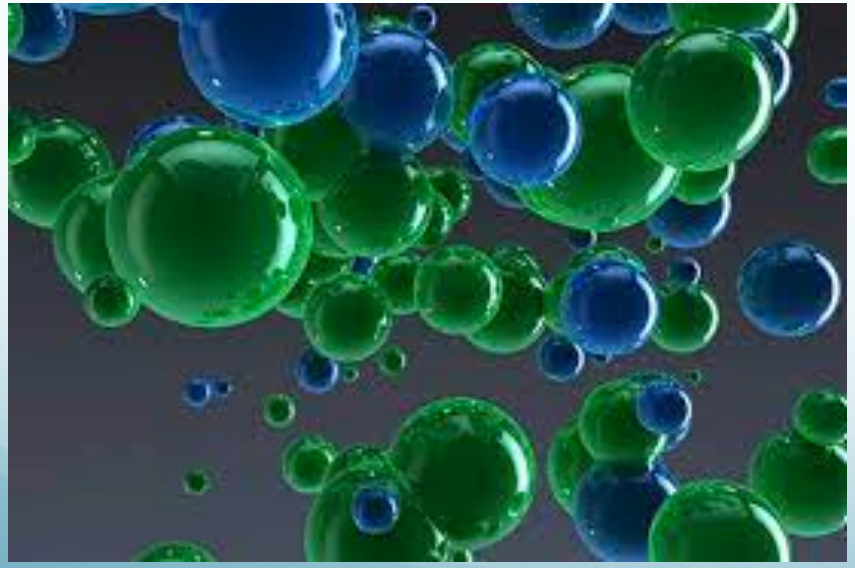

$$\frac{\partial \rho}{\partial t} + \nabla \cdot [\rho \mathbf{v}] = 0$$

$$\frac{\partial (\rho \mathbf{v})}{\partial t} + \nabla \cdot [\rho \mathbf{v}\mathbf{v} - \mathbf{B}\mathbf{B} + \mathsf{P}^*] = 0$$

$$\frac{\partial E}{\partial t} + \nabla \cdot [(E + P^*)\mathbf{v} - \mathbf{B}\,(\mathbf{B} \cdot \mathbf{v})] = 0$$

$$\frac{\partial \mathbf{B}}{\partial t} - \nabla \times (\mathbf{v} \times \mathbf{B}) = 0$$

$$P^* = P + \frac{\mathbf{B} \cdot \mathbf{B}}{2}$$

$$E = P/(\gamma - 1) + \frac{\rho(\mathbf{v} \cdot \mathbf{v})}{2} + \frac{\mathbf{B} \cdot \mathbf{B}}{2}$$

turbulence development

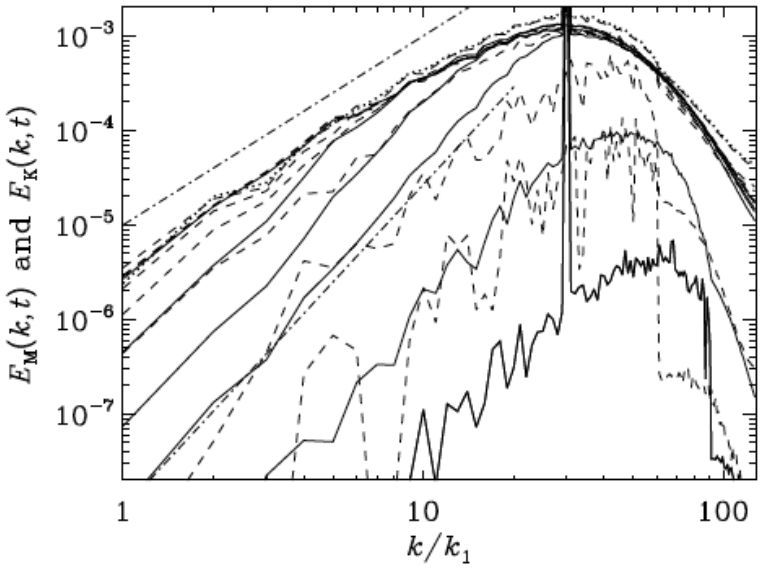

$$\frac{D\rho}{Dt} = -\rho\boldsymbol{\nabla}\cdot\mathbf{u},$$
$$\rho\frac{D\mathbf{u}}{Dt} = (\boldsymbol{\nabla}\times\mathbf{b})\times\mathbf{b} - c_{\rm s}^2\boldsymbol{\nabla}\rho + \boldsymbol{\nabla}\cdot(2\rho\nu\mathbf{S}),$$
$$\frac{\partial\mathbf{A}}{\partial t} = \mathbf{u}\times\mathbf{b} + \eta\nabla^2\mathbf{A},$$

where $D/Dt = \partial/\partial t + \mathbf{u}\cdot\boldsymbol{\nabla}$ is the advective derivative, t is the conformal time, ρ is the density, $\mathbf{u}$ is the bulk velocity, $\mathsf{S}_{ij} = \frac{1}{2}(u_{i,j} + u_{j,i}) - \frac{1}{3}\delta_{ij}\boldsymbol{\nabla}\cdot\mathbf{u}$ is the rate-of-strain tensor, ν is the viscosity, and η is the magnetic diffusivity.

Kahniashvili et al. 2010

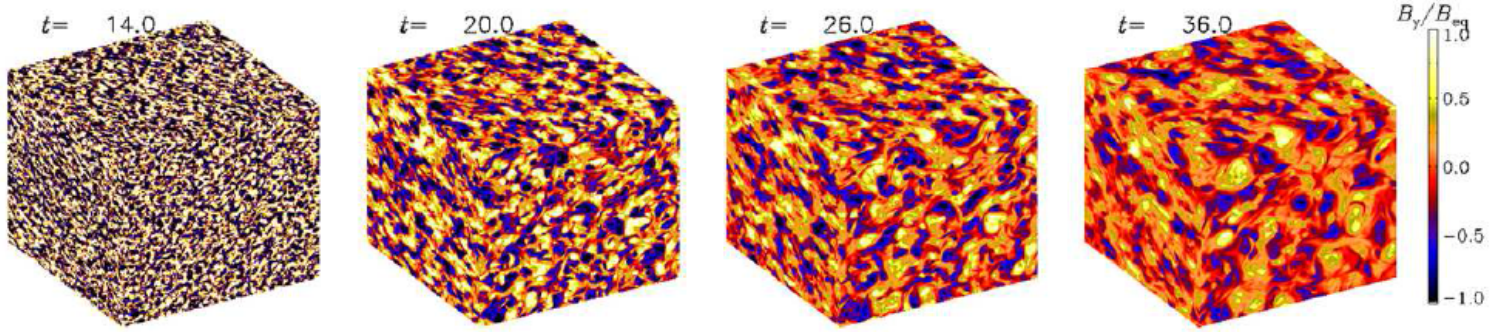

FIG. 2: Evolution of the turbulent magnetic field after turning off the forcing at time $t = 14\,t_1$. The B_y component is shown on the periphery of the computational domain.

our universe is almost perfect conductor

magnetically dominant

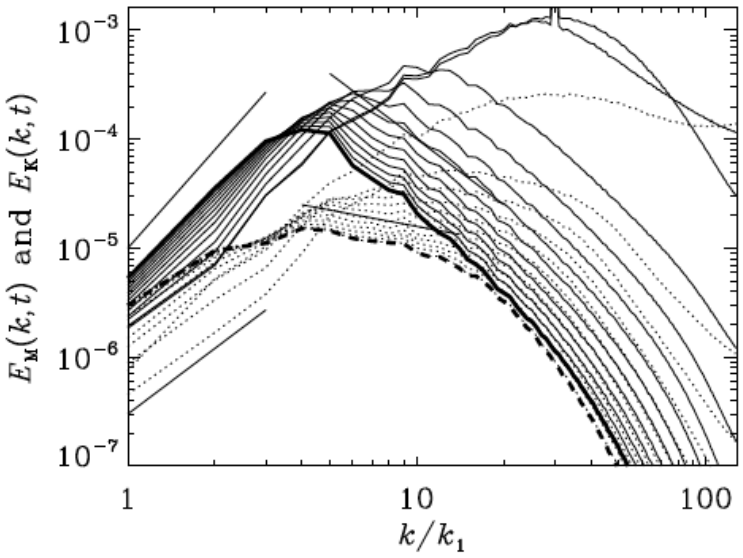

FIG. 5: Magnetic (solid) and kinetic (dashed) energy spectra in 12 regular time intervals of $4\,t_1$ after having turned off the forcing, with (smoothed) spectra at $k = 50k_1$ decreasing as t increases. $\nu = \eta = 10^{-4}$ in units of $(k_1^2 t_1)^{-1}$. The straight lines have slopes 3, 2, -2, and $-1/2$, with the first two near $k = k_1$ and the last two near $k = 10k_1$. Thickest lines (solid and dashed) indicate the last time, which is $44\,t_1$ since turning off the forcing. The intermediate thickness solid line, the highest or almost highest line for $k/k_1 > 10$, is the initial magnetic spectrum for this computation.

kinetically dominant

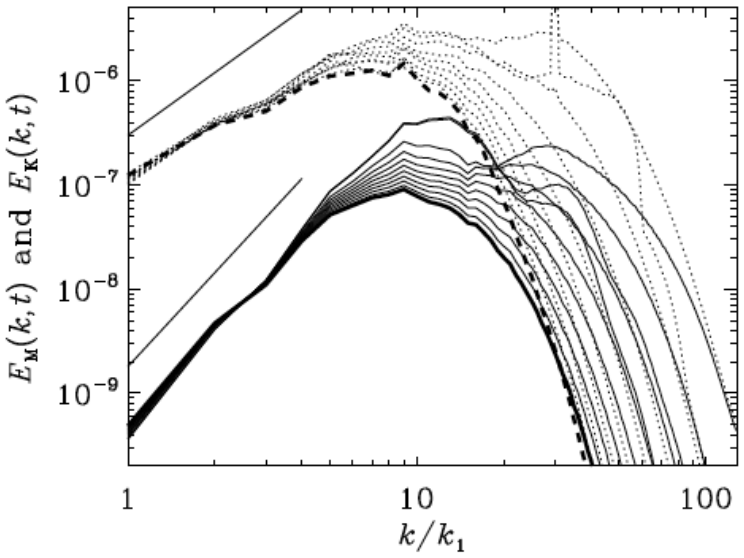

FIG. 6: Same as Fig. 5, but for a case where the initial magnetic field had a k^4 spectrum close to equipartition with the velocity field, and then the forcing was turned off. Results are shown for nine times at intervals of $6\,t_1$. $\nu = \eta = 10^{-4}$ in units of $(k_1^2 t_1)^{-1}$. The straight lines have slopes 2 and 3. Thickest lines (solid and dashed) indicate the last time, which is $48\,t_1$ since turning off the forcing. The intermediate thickness solid line, the highest solid line for $5 < k/k_1 < 10$, is the initial magnetic spectrum for this computation.

Kahniashvili et al. 2010

high resolution 3D compressible MHD simulations - decay

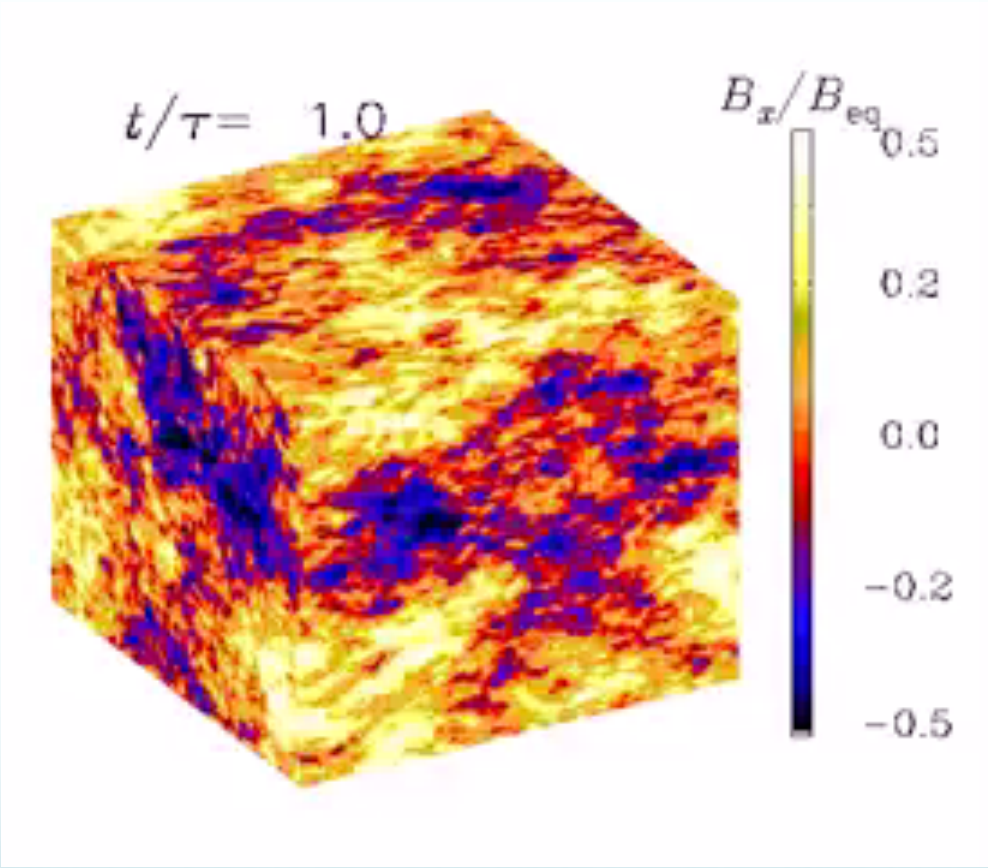

Brandenburg et al. 2015

inverse transfer?

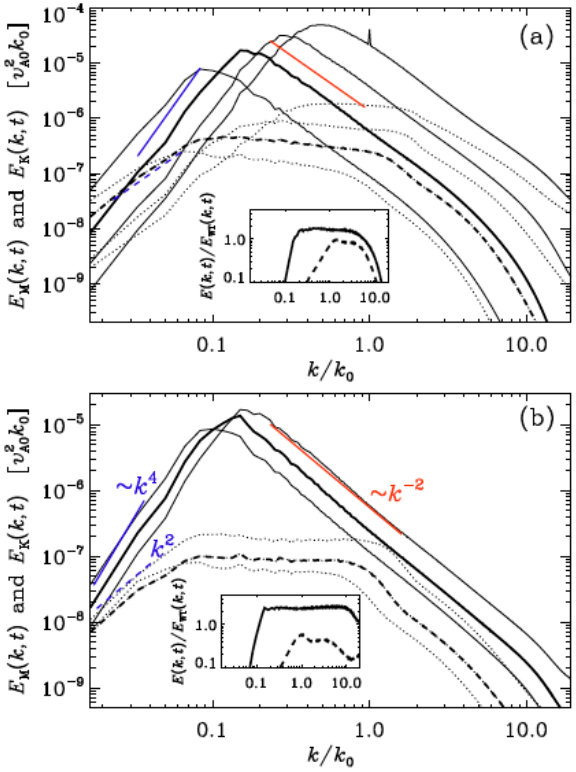

FIG. 1: (Color online) (a) Magnetic (solid lines) and kinetic (dashed lines) energy spectra for Run A at times $t/\tau_A = 18$, 130, 450, and 1800; the time $t/\tau_A = 450$ is shown as bold lines. The straight lines indicate the slopes k^4 (solid, blue), k^2 (dashed, blue), and k^{-2} (red, solid). (b) Same for Run B, at $t/\tau_A = 540$, 1300, and 1800, with $t/\tau_A = 1300$ shown as bold lines. The insets show E_M and E_K compensated by E_{WT}.

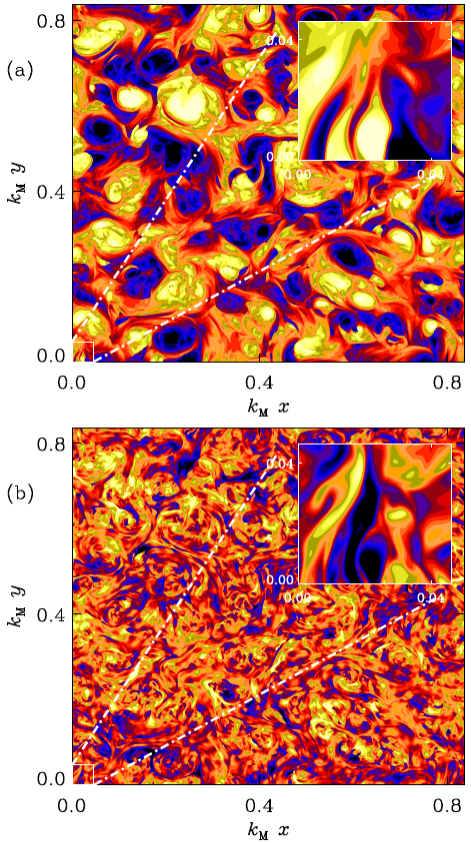

FIG. 2: (Color online) Contours of (a) $B_z(x,y)$ and (b) $u_z(x,y)$ for Run A. The insets show a zoom into the small square in the lower left corner.

Brandenburg, Kahniashvili, Tevzadze 2015

classes of turbulences

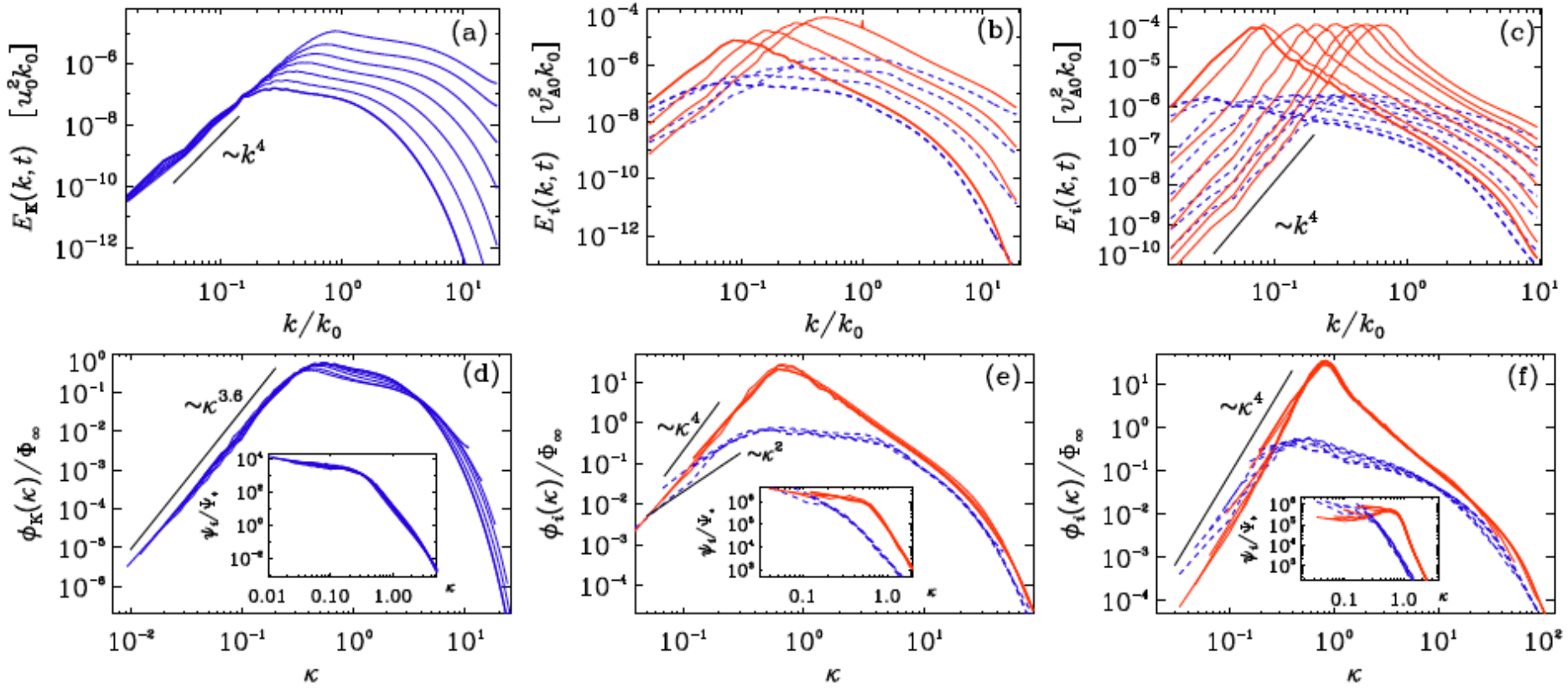

Brandenburg & Kahniashvili 2017

classes of MHD turbulence

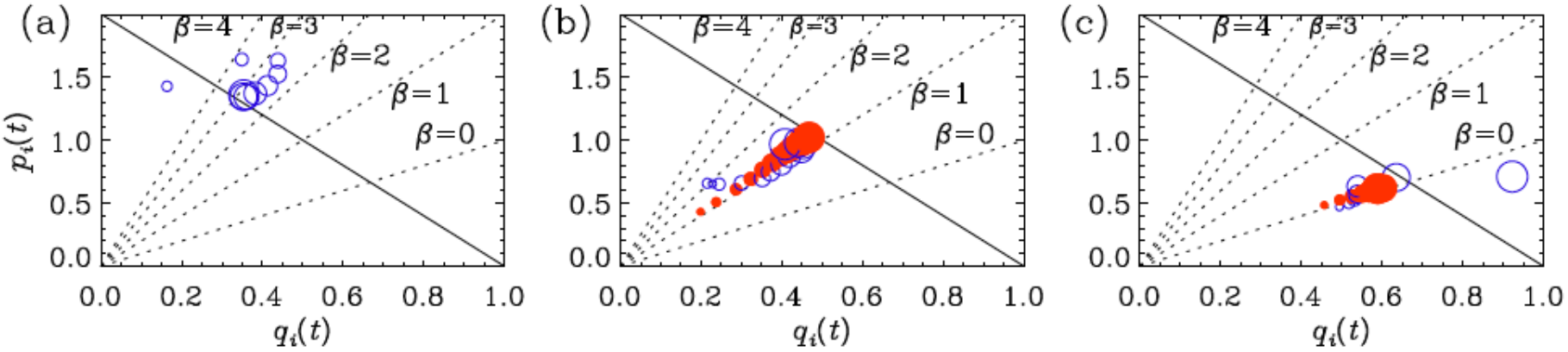

FIG. 2: pq diagrams for cases (i)–(iii). Open (closed) symbols correspond to $i = \mathrm{K}$ (M) and their sizes increase with time.

TABLE I: Scaling exponents and relation to physical invariants and their dimensions.

β	p	q	inv.	dim.
4	$10/7 \approx 1.43$	$2/7 \approx 0.286$	$\mathcal{L}$	$[x]^7[t]^{-2}$
3	$8/6 \approx 1.33$	$2/6 \approx 0.333$		
2	$6/5 = 1.20$	$2/5 = 0.400$		
1	$4/4 = 1.00$	$2/4 = 0.500$	$\langle A_{2\mathrm{D}}^2 \rangle$	$[x]^4[t]^{-2}$
0	$2/3 \approx 0.67$	$2/3 \approx 0.667$	$\langle \boldsymbol{A} \cdot \boldsymbol{B} \rangle$	$[x]^3[t]^{-2}$
-1	$0/2 = 0.00$	$2/1 = 1.000$		

$$\mathcal{E}_i(t) \sim t^{-p_i} \text{ for } i = \mathrm{K} \text{ or } \mathrm{M}$$

$$\xi \propto t^q,$$

Brandenburg & Kahniashvili 2017

inflationary magnetogensis

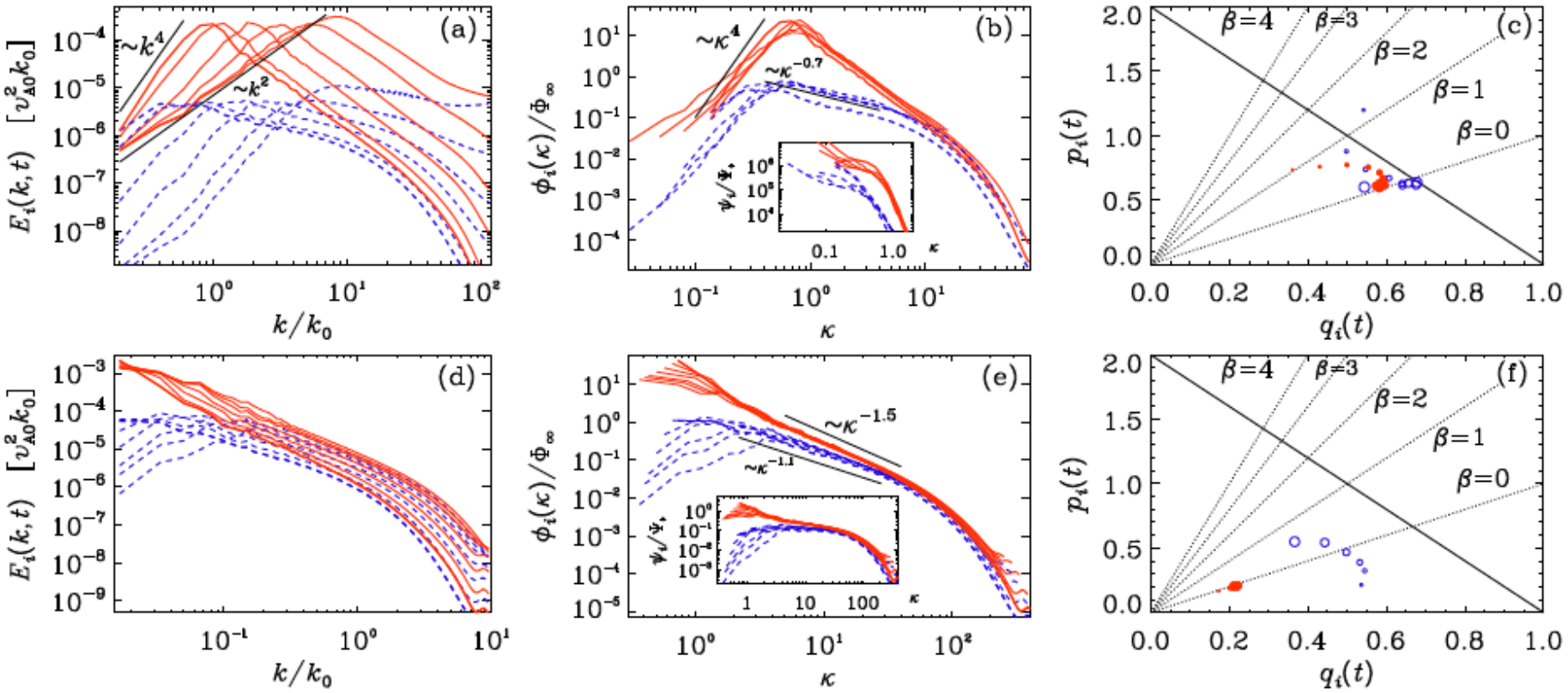

FIG. 3: E_M (solid) and E_K (dashed) in MHD with fractional helicity and $\alpha = 2$ (a), as well as full helicity and $\alpha = -1$ (d), together with compensated spectra (b,e) and the pq diagrams (c,f).

Brandenburg & Kahniashvili 2017

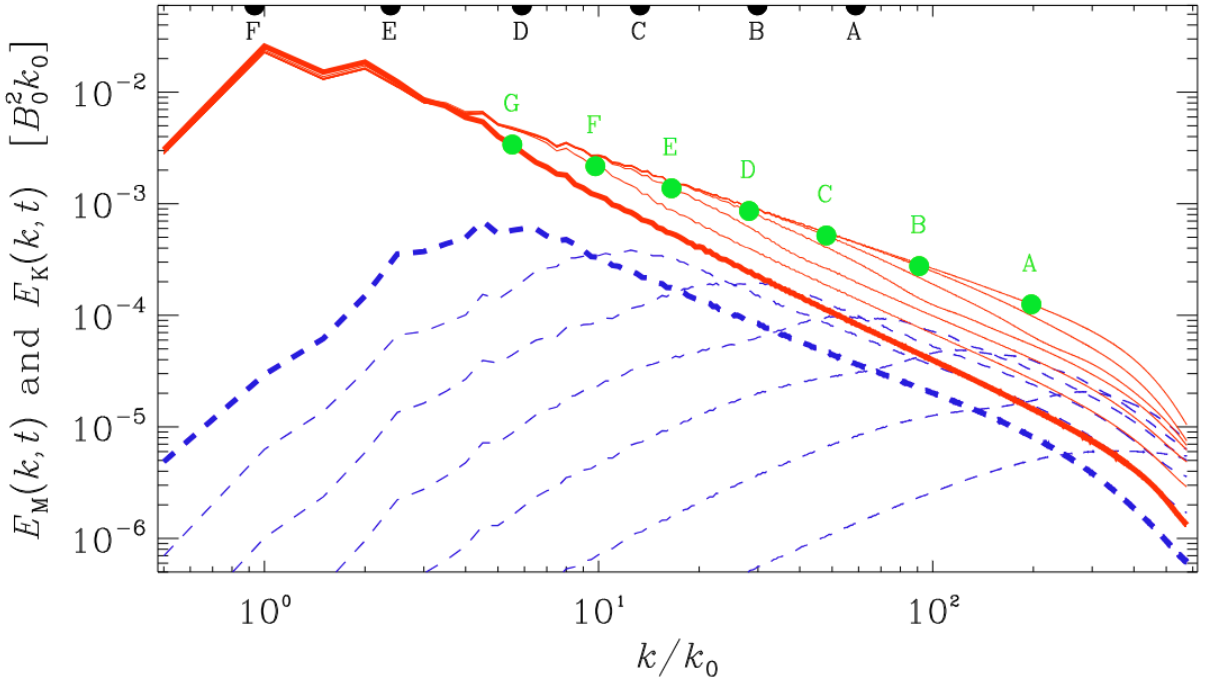

$$k_\star(t) \approx \xi_{\rm M}(t)\,(\eta_{\rm turb} t)^{-1/2} \approx (u_{\rm rms} k_{\rm M} t/3)^{-1/2},$$

Figure 7: Magnetic (red) and kinetic (blue) energy spectra at early times after having initialized the magnetic field with a scale-invariant spectrum for $k > k_0$ and a k^4 spectrum for $k < k_0$. Here, k_0 is the wavenumber of the peak, which was chosen to be twice as big as the smallest wavenumber in the domain. The green symbols on the red lines denote the position of $k_\star(t)$, as given in Eq. (29), while the black symbols on the upper abscissa denote the location of the horizon wavenumber $k_{\rm hor}(t)$. The letters A–G on the spectra and the upper abscissa correspond to the same times. Adapted from Brandenburg et al. (2018).

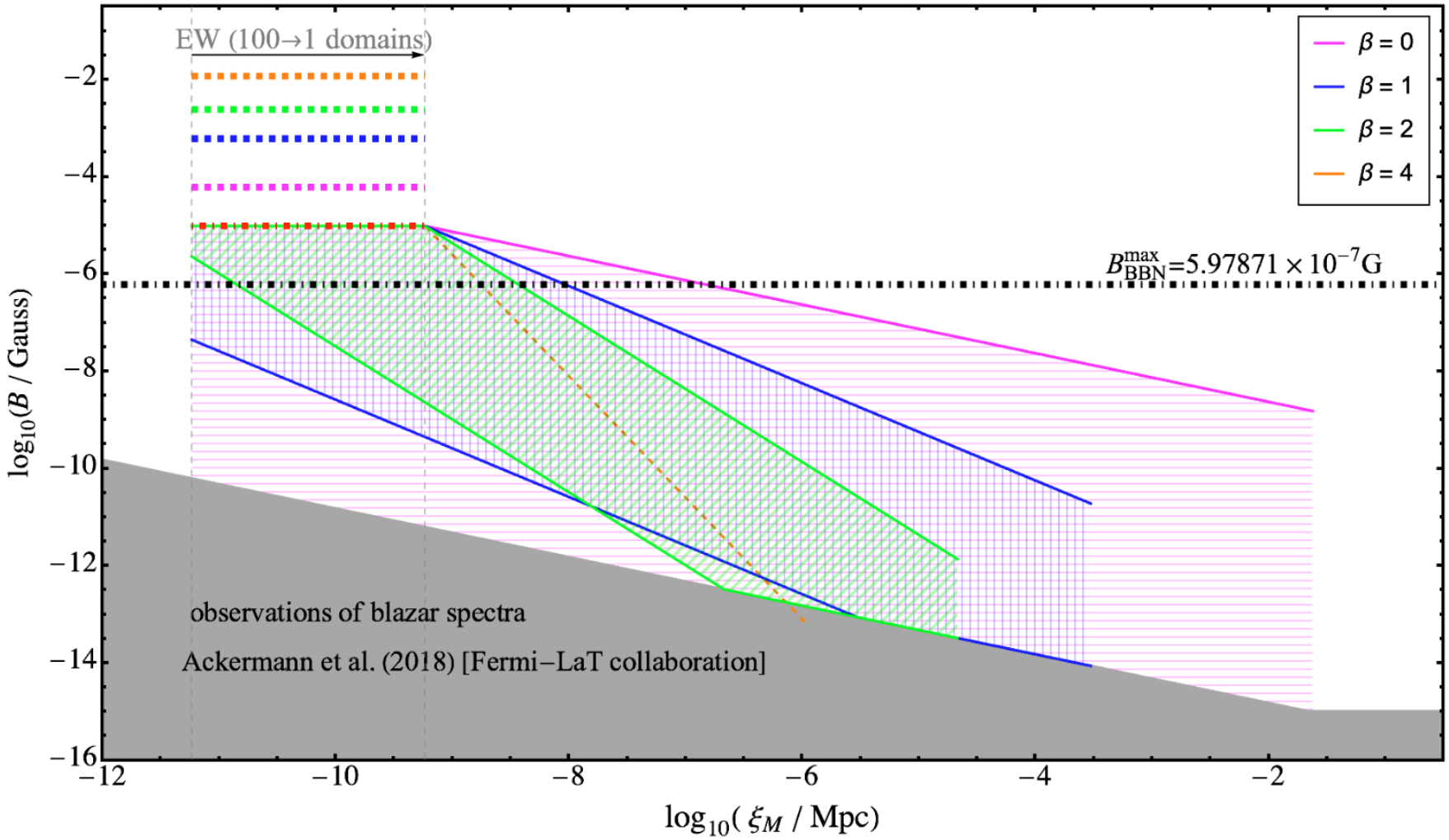

Figure 8: BBN bounds on the electroweak phase transition initial field strength marked by horizontal dashed lines. Based on an initial bound of $\rho_B/\rho_{\rm rad} = 1$, all trajectories for this case are *below* the Ackermann bound by recombination. Courtesy: Emma Clarke

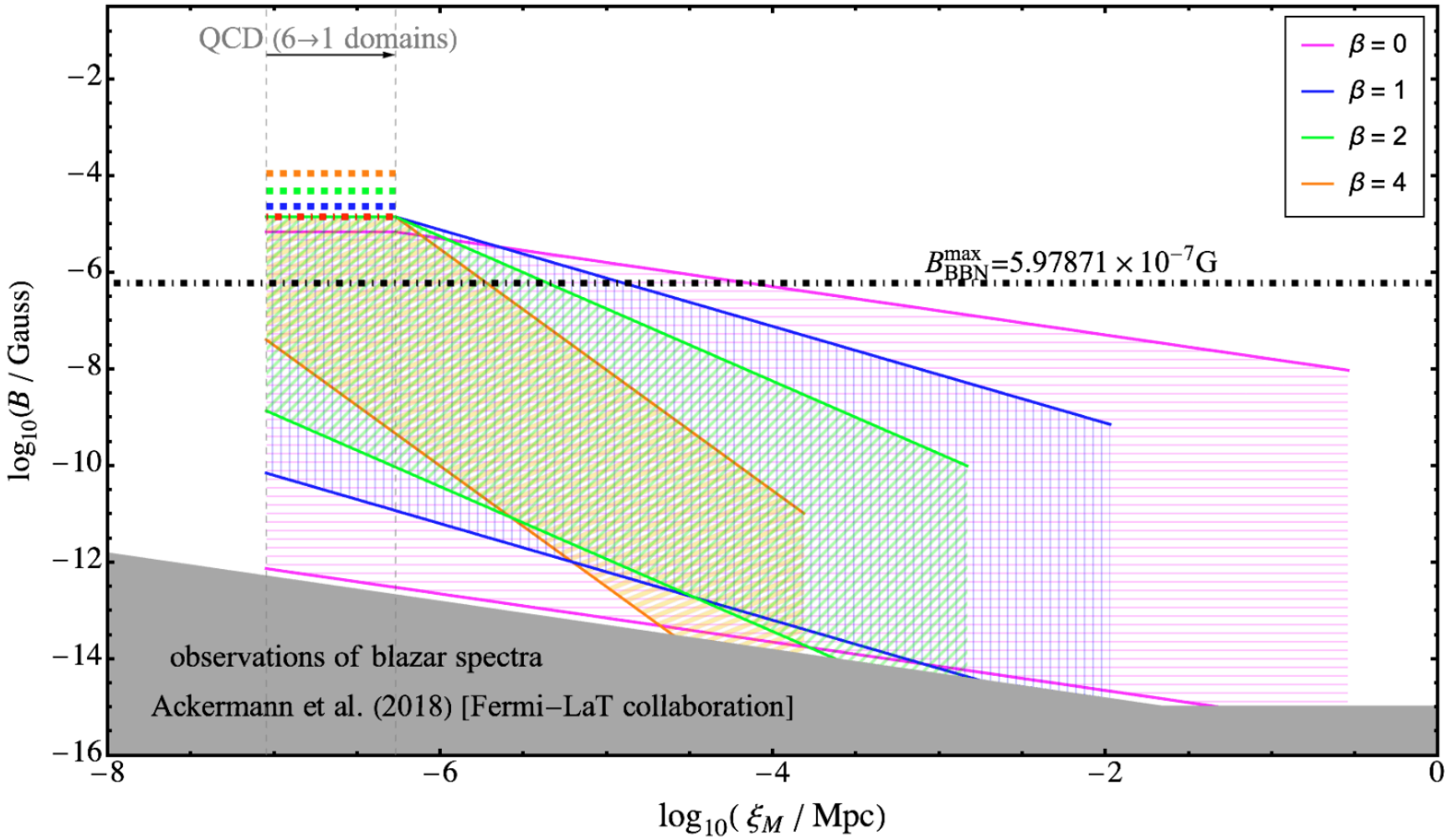

Figure 9: BBN bounds on the QCD phase transition generated initial field strength marked by horizontal dashed lines. For the non-helical cases, the initial energy density bound is more constraining than the BBN bound. Courtesy: Emma Clarke

evolution through structure formation

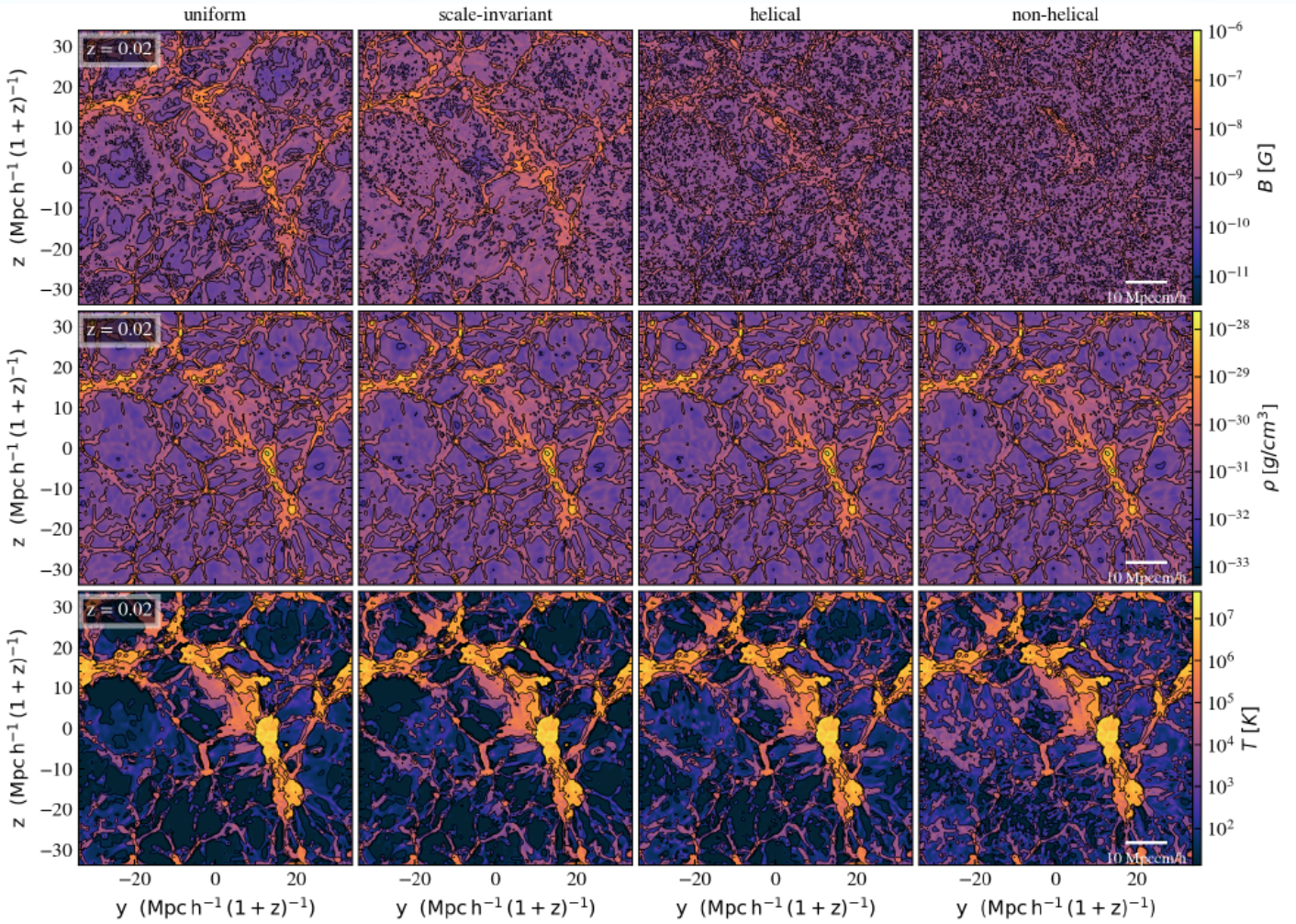

Figure 3. The contoured slices through the center of the simulated box at $z = 0.02$. The top, middle, and bottom panels show the magnetic field, density and temperature slices correspondingly. The overplotted contour lines mark the regions with a certain field strength and the range of the field values are set according to the minimum and maximum of the annotated fields.

Mtchedlidze et al, 2021

late time evolution

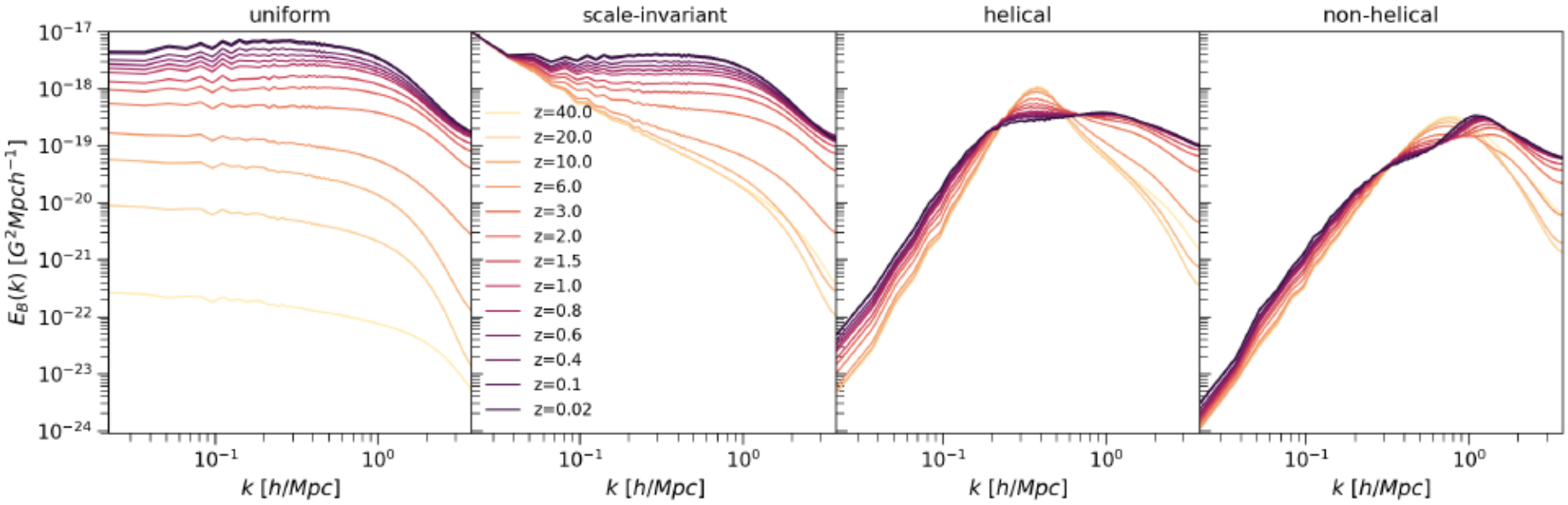

Figure 6. Redshift evolution of magnetic power spectra; from left to right: the uniform, scale-invariant, helical and non-helical seedings.

Mtchedlidze et al, 2021

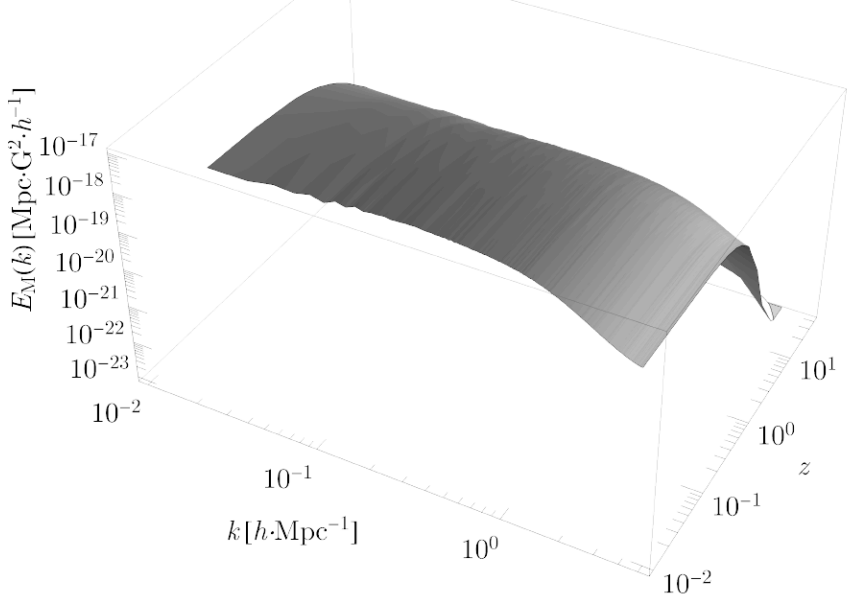

(a) Uniform spectrum.

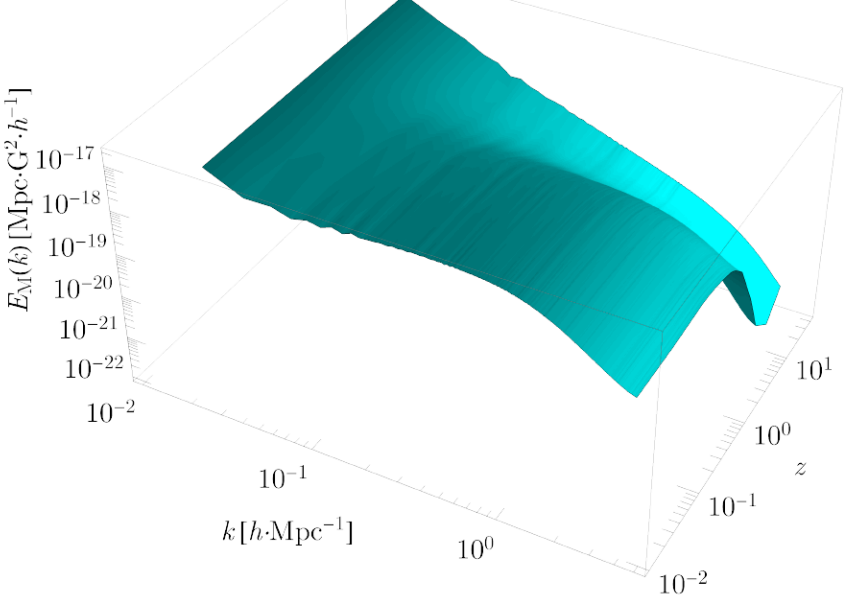

(b) Scale-invariant spectrum.

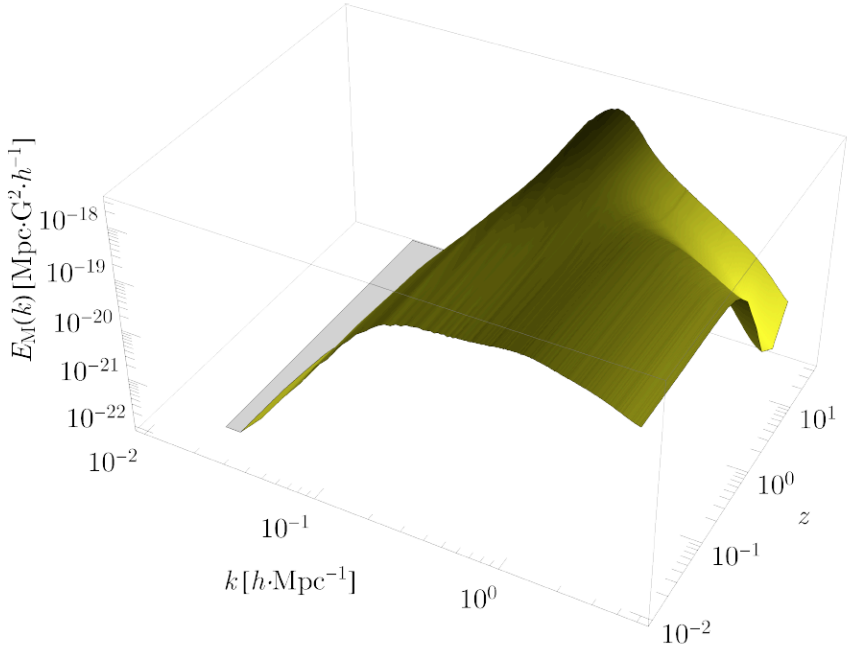

(c) Helical spectrum.

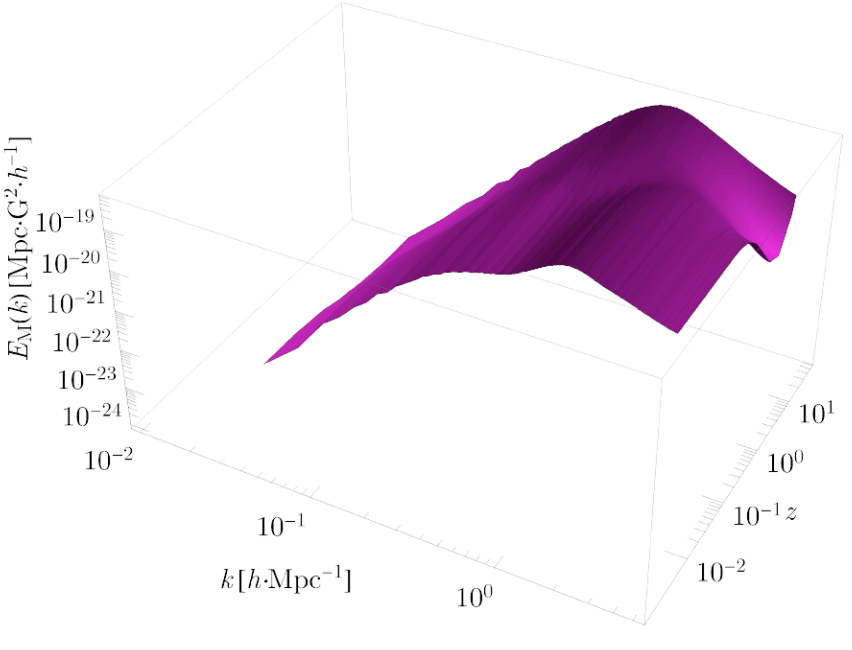

(d) Non-helical spectrum.

conclusions

- The high conductivity of primordial plasma insures possibility of hydro and magneto-hydrodynamics turbulence development in the early universe
- Turbulence experiences decay through the expansion of the universe
- Primordial MHD turbulence is a plausible explanation of the observed magnetic fields in galaxies, clusters, and voids (if confirmed)
- Primordial turbulence signatures include:
  - gravitational waves
  - cosmic microwave background fluctuations
  - effects of the matter power spectrum (large scale structure)

Thank You
Questions?